Design of Link Slabs: Material and Structural Considerations

Final Report
July 2022

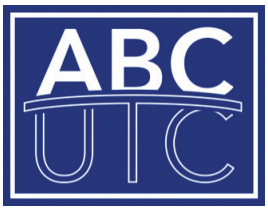

Sponsored by
Accelerated Bridge Construction
University Transportation Center

U.S. Department of Transportation
Office of the Assistant Secretary for
Research and Technology

IOWA STATE UNIVERSITY
Institute for Transportation

About the ABC-UTC

The Accelerated Bridge Construction University Transportation Center (ABC-UTC) is a Tier 1 UTC sponsored by the U.S. Department of Transportation Office of the Assistant Secretary for Research and Technology (USDOT/OST-R). The mission of ABC-UTC is to reduce the societal costs of bridge construction by reducing the duration of work zones, focusing special attention on preservation, service life, construction costs, education of the profession, and development of a next-generation workforce fully equipped with ABC knowledge.

About the Bridge Engineering Center

The mission of the Bridge Engineering Center (BEC), which is part of the Institute for Transportation (InTrans) at Iowa State University, is to conduct research on bridge technologies to help bridge designers/owners design, build, and maintain long-lasting bridges. The mission of InTrans is to save lives and improve economic vitality through discovery, research innovation, outreach, and the implementation of bold ideas.

Iowa State University Nondiscrimination Statement

Iowa State University does not discriminate on the basis of race, color, age, ethnicity, religion, national origin, pregnancy, sexual orientation, gender identity, genetic information, sex, marital status, disability, or status as a US veteran. Inquiries regarding nondiscrimination policies may be directed to the Office of Equal Opportunity, 3410 Beardshear Hall, 515 Morrill Road, Ames, Iowa 50011, telephone: 515-294-7612, hotline: 515-294-1222, email: eooffice@iastate.edu.

Disclaimer Notice

The contents of this report reflect the views of the authors, who are responsible for the facts and the accuracy of the information presented herein. The opinions, findings and conclusions expressed in this publication are those of the authors and not necessarily those of the sponsors.

The sponsors assume no liability for the contents or use of the information contained in this document. This report does not constitute a standard, specification, or regulation.

The sponsors do not endorse products or manufacturers. Trademarks or manufacturers' names appear in this report only because they are considered essential to the objective of the document.

Quality Assurance Statement

The Federal Highway Administration (FHWA) provides high-quality information to serve Government, industry, and the public in a manner that promotes public understanding. Standards and policies are used to ensure and maximize the quality, objectivity, utility, and integrity of its information. The FHWA periodically reviews quality issues and adjusts its programs and processes to ensure continuous quality improvement.

Technical Report Documentation Page

1. Report No. ABC-UTC-2016-C2-ISU04-Final	**2. Government Accession No.**	**3. Recipient's Catalog No.**
4. Title and Subtitle **Design of Link Slabs: Material and Structural Considerations**		**5. Report Date** July 2022 6. Performing Organization Code
7. Author(s) Behrouz Shafei (orcid.org/0000-0001-5677-6324) and Rizwan Karim (orcid.org/0000-0003-4130-568X)		**8. Performing Organization Report No.**
9. Performing Organization Name and Address Bridge Engineering Center Iowa State University 2711 South Loop Drive, Suite 4700 Ames, IA 50010-8664		**10. Work Unit No. (TRAIS)** **11. Contract or Grant No.** 69A3551747121
12. Sponsoring Organization Name and Address Accelerated Bridge Construction University Transportation Center Florida International University 10555 W. Flagler Street, EC 3680 Miami, FL 33174 U.S. Department of Transportation Office of the Assistant Secretary for Research and Technology and Federal Highway Administration 1200 New Jersey Avenue, SE Washington, DC 20590		**13. Type of Report and Period Covered** Final Report (January 2020–December 2021) **14. Sponsoring Agency Code**
15. Supplementary Notes Visit https://abc-utc.fiu.edu/ for other ABC reports.		

16. Abstract

A common technique in accelerated bridge construction (ABC) is the use of prefabricated bridge elements and systems (PBES). The bridge components are built outside of the construction area, transported to the site, and then rapidly installed. This helps significantly reduce the time required for concrete placement and curing as well as formwork erection and removal. Another benefit to using PBES is improved quality control. Damage due to weather is also minimized because elements are built in a controlled environment. However, an open question is how to address the long-term performance and durability concerns associated with the joints that connect high-quality bridge elements.

To address this question, one approach that has gained significant attention is to eliminate the joints through the addition of link slabs. The current project built on the outcome of experimental tests and numerical simulations performed on link slabs at Iowa State University for a previous ABC-UTC-sponsored research project to explain their structural performance under various loading conditions. A short course module was developed to provide the design guidelines and practical recommendations necessary to properly implement link slabs in jointless bridges. The course covers a range of material and structural aspects, including alternative concrete and rebar choices, crack criteria, bonding/debonding requirements, and reinforcement details.

17. Key Words accelerated bridge construction—expansion joints—links slabs		**18. Distribution Statement** No restrictions.	
19. Security Classification (of this report) Unclassified.	**20. Security Classification (of this page)** Unclassified.	**21. No. of Pages** 58	**22. Price**

Form DOT F 1700.7 (8-72) **Reproduction of completed page authorized**

(this page is intentionally left blank)

Design of Link Slabs: Material and Structural Considerations

Final Report

July 2022

Principal Investigator
Behrouz Shafei, Associate Professor
Bridge Engineering Center, Institute for Transportation
Iowa State University

Research Assistant
Rizwan Karim

Authors
Behrouz Shafei and Rizwan Karim

Sponsored by
Accelerated Bridge Construction University Transportation Center

A report from
Bridge Engineering Center and Institute for Transportation
Iowa State University
2711 South Loop Drive, Suite 4700
Ames, IA 50010-8664
Phone: 515-294-8103 / Fax: 515-294-0467
https://intrans.iastate.edu/

DISCLAIMER

The contents of this report reflect the views of the authors, who are responsible for the facts and the accuracy of the information presented herein. This document is disseminated in the interest of information exchange. The report is funded, partially or entirely, by a grant from the U.S. Department of Transportation's University Transportation Program. However, the U.S. Government assumes no liability for the contents or use thereof.

TABLE OF CONTENTS

LIST OF FIGURES

ACKNOWLEDGMENTS

This project was supported by the Accelerated Bridge Construction University Transportation Center (ABC-UTC at https://abc-utc.fiu.edu/) at Florida International University (FIU) as the lead institution, with Iowa State University, the University of Nevada-Reno, the University of Oklahoma, and the University of Washington as partner institutions. The authors would like to acknowledge the support of the ABC-UTC.

The research team would like to extend special appreciation to the ABC-UTC and the U.S. Department of Transportation Office of the Assistant Secretary for Research and Technology for funding this project.

The authors would like to thank Doug Wood, Shahin Hajilar, Michael Dopko, and Brent Phares for their laboratory and technical assistance. Thanks should also be given to the many state agency representatives who provided feedback on the content presented in this report.

INTRODUCTION

Background

The application of accelerated bridge construction (ABC) has increased significantly due to the unique advantages of bridges built using ABC techniques, including the short duration of construction and the high quality of prefabricated bridge elements and systems (PBES) commonly used in ABC. Because the bridge components are built outside of the construction area, transported to the site, and then rapidly installed, the time required for concrete placement and curing as well as formwork erection and removal is significantly reduced. By decreasing the construction time from months to days, ABC techniques contribute to work zone safety by minimizing the on-site activities that can cause accidents for construction workers and motorists. Moreover, the use of PBES improves quality control, as bridge elements are built in a controlled environment. The improved product quality achieved through PBES enhances the durability and performance of bridges during their design life.

Despite major advances in the design and construction of the prefabricated bridge elements for ABC applications, the long-term performance and durability of bridges constructed using ABC techniques remain a concern because of the expansion joints used to connect the high-quality bridge elements. These expansion joints play a critical role in accommodating unrestrained deformations in adjacent spans due to thermal expansion and traffic loads. The existing types of expansion joints, however, deteriorate rapidly and require significant maintenance effort. While various strategies have been successfully developed to improve the integral abutments used for ABC applications, no established approach is available that can replace the current expansion joints used between bridge spans. One approach to address this issue is to eliminate expansion joints through revised design strategies. A key strategy that has gained significant attention is the use of link slabs to eliminate expansion joints.

Scope and Objectives

This project followed a systematic plan to develop a short course module on link slabs. The course builds on the outcome of experimental tests and numerical simulations performed on link slabs at Iowa State University for a previous ABC-UTC-sponsored research project (Shafei et al. 2018, Karim and Shafei 2021a) to explain their structural performance under various loading conditions.

The course provides the design guidelines and practical recommendations necessary to properly implement link slabs in jointless bridges. The course covers a range of material and structural aspects, including alternative concrete and rebar choices, crack criteria, bonding/debonding requirements, and reinforcement details. The course thus creates a unique resource for a wide group of practicing bridge engineers, researchers in the bridge engineering domain, and graduate and undergraduate students.

This report presents the content of the short course module developed for this project.

EXPANSION JOINTS VERSUS LINK SLABS

Expansion Joints

Expansion joints are commonly included in bridge structures to accommodate thermal movements and release stresses resulting from possible support constraints.

The following problems are associated with expansion joints (Lárusson 2013, Ho and Lukashenko 2011):

- Significant maintenance effort and cost required for expansion joints
- Corrosion of substructure, including girder ends, bearings, and piers (Figures 1 and 2)
- Possible bridge closures, traffic disruptions, and indirect costs and consequences

Ho and Lukashenko 2011 (from Lárusson 2013)

Figure 1. Corroded substructure under an expansion joint

The Crittenden Press 2012 (from Lárusson 2013)

Figure 2. Corroded expansion joint from the bottom

Link Slabs

Link slabs, an example of which is illustrated in Figure 3, are included in bridge decks to eliminate expansion joints and create a continuous deck system.

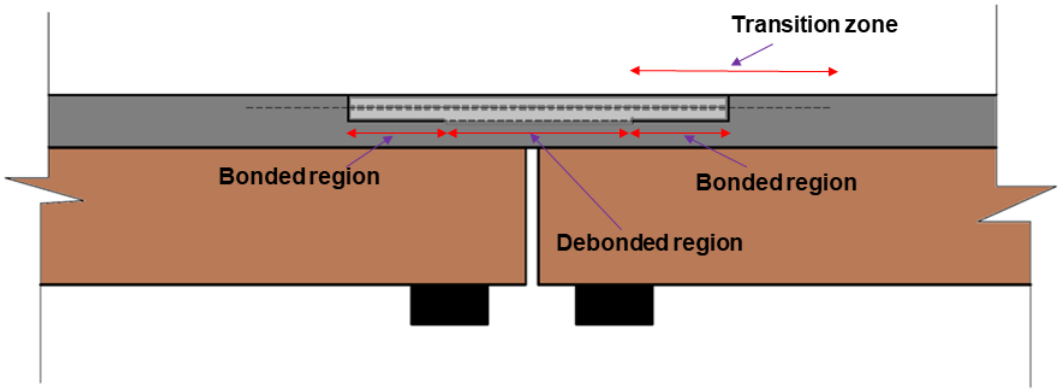

Figure 3. Link slab

Link slabs include the following regions:

- **Debonded Region**. A link slab's length of 2.5% to 10.0% (of the adjacent span) is often debonded from the underlying deck to evenly distribute the bending moment. Based on the literature, the recommended debonded length is 5.0%. Debonding is provided by either a plastic sheet or a roofing paper, depending on the surface type.

- **Bonded Region**. This refers to a portion of a link slab that has a dense reinforcement with no debonding. The rebar density helps with transferring the strains/stresses from the deck to the link slab's debonded region.

- **Transition Zone**. This refers to the bonded region, plus the region through which the link slab's rebars are extended to the bridge deck.

MATERIAL SELECTION

Expected Material Characteristics

The material choices appropriate for link slabs include various cementitious materials. Specifically, engineered cementitious composite (ECC), ultra-high performance concrete (UHPC), and fiber-reinforced concrete (FRC) are promising choices.

In terms of key material characteristics, it is desirable to use a cementitious material that can deliver minimal cracks with crack bridging capabilities under external loads. Additionally, a material with high ductility and tension stiffening properties is a suitable choice.

As for embedded reinforcement, both steel and glass fiber-reinforced polymer (GFRP) bars can be considered.

The remainder of this chapter offers more detail about the three cementitious materials noted above and the considerations related to embedded reinforcement.

Cementitious Materials

Engineered Cementitious Composites

After the use of conventional concrete with embedded steel reinforcement in very first link slabs (e.g., Wing and Kowalsky 2005), ECC was considered (e.g., Li and Lepech 2009) due to the following advantages (Figure 4):

- Reduction in the number of rebars required
- Improvement in the main durability properties
- Provision of strain hardening capabilities
- Formation of fine cracks instead of large ones
- Delivery of an ultimate strain as high as 5%

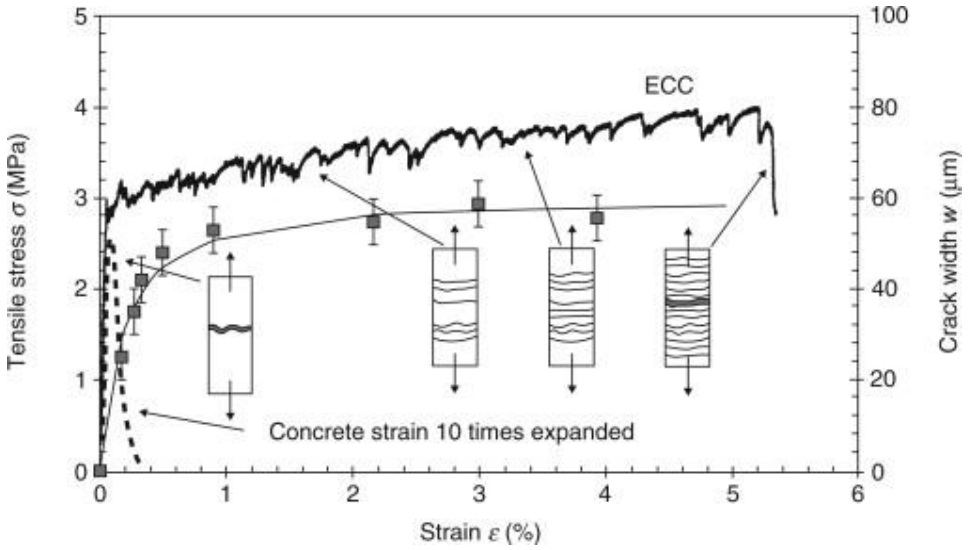

1 MPa = 0.145 ksi; 100 μm = 0.004 in

Li 2007

Figure 4. Tensile stress and crack width versus strain for ECC

Investigations performed on ECC link slabs (e.g., Kim et al. 2005, Li and Lepech 2009) have found the following:

- Under monotonic loads, strains in concrete link slabs were higher than those in ECC link slabs. This was primarily attributed to strain hardening and microcracking in ECC.

- Under cyclic loads, both concrete and ECC link slabs showed no degradation in stiffness after 100,000 cycles. However, the crack widths in concrete link slabs were (on average) 10 times larger than those in ECC link slabs (Figure 5).

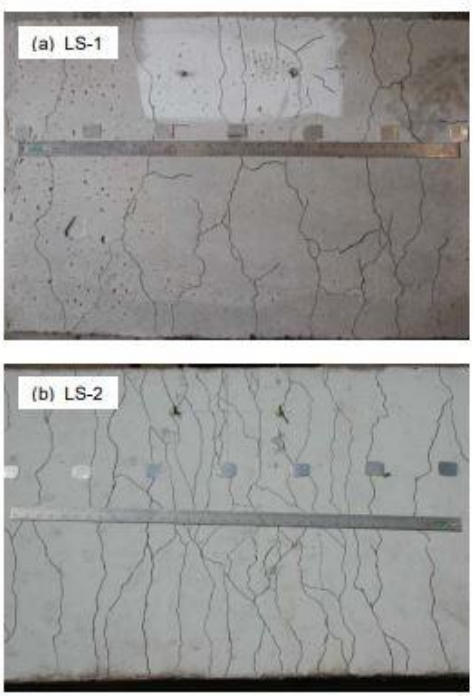

Li et al. 2003

Figure 5. Crack widths in concrete link slab (top) versus ECC link slab (bottom)

Ultra-High Performance Concrete

UHPC is known to offer superior mechanical and durability properties (Graybeal 2013, Karim et al. 2019). The use of UHPC for link slabs can deliver well-distributed microcracks, further to crack bridging capabilities, owing to the presence of steel fibers (Figure 6).

UHPC has a compressive strength in the range of 150 MPa (22 ksi) and can offer an ultimate strain capacity of 0.007 to 0.010.

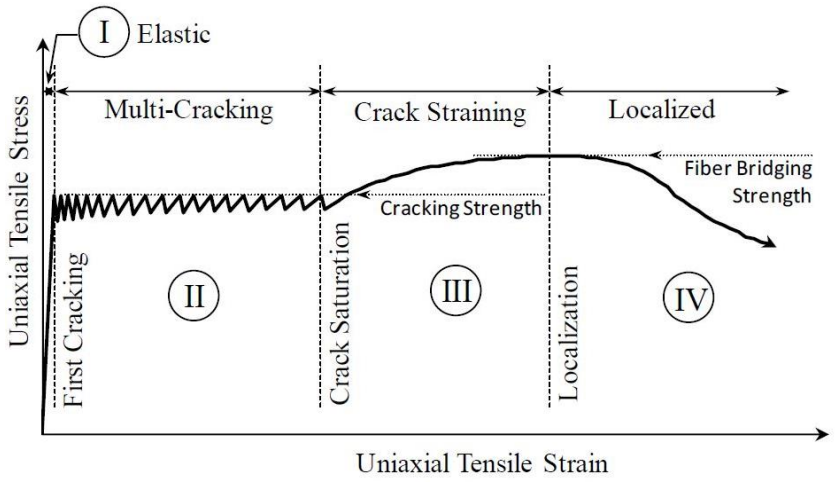

Russell and Graybeal 2013

Figure 6. Uniaxial tensile stress versus uniaxial tensile strain for UHPC

Investigations performed on UHPC link slabs have found the following:

- The New York State Department of Transportation (NYSDOT) has experimented with the use of UHPC in link slabs.
- Link slabs made with UHPC have been performing well, with no visible cracks (Figure 7).
- The durability and resistance against chloride ions and deicing agents offer additional value to the use of UHPC for link slabs.

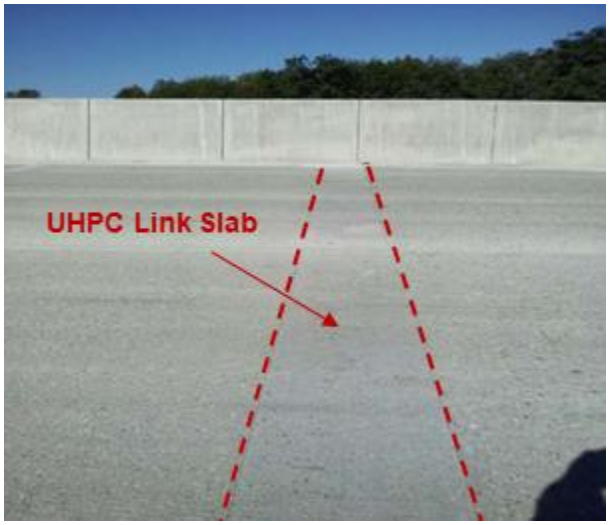

After Royce 2016, with annotations added

Figure 7. Use of UHPC in link slabs

Fiber-Reinforced Concrete

Adding discontinuous fibers to concrete results in a composite material with improved properties in both fresh and hardened states. The use of synthetic fibers in FRC helps reduce their cost and increase their corrosion resistance compared to metallic fibers.

Among the variety of synthetic fibers available, polypropylene (PP), alkali-resistant (AR) glass, and polyvinyl alcohol (PVA) fibers are deemed promising choices (Dopko et al. 2018, Shafei et al. 2021). These types of fibers are shown in Figure 8.

Figure 8. PP fibers (left), AR glass fibers (center), PVA fibers (right)

Shafei et al. (2018) tested the flexural performance of FRC mixtures containing different volumes of PP, AR glass, and PVA fibers. Three beam specimens were cast and tested for each mixture, and average performance parameters were computed. The testing apparatus is shown in Figure 9, cracked beam specimens are shown in Figure 10, and an example of the results is shown in Figure 11.

Shafei et al. 2018, Bridge Engineering Center

Figure 9. Testing apparatus for flexural strength of beam specimens

Shafei et al. 2018, Bridge Engineering Center

Figure 10. Single crack (left) and double crack (right) in beam specimens

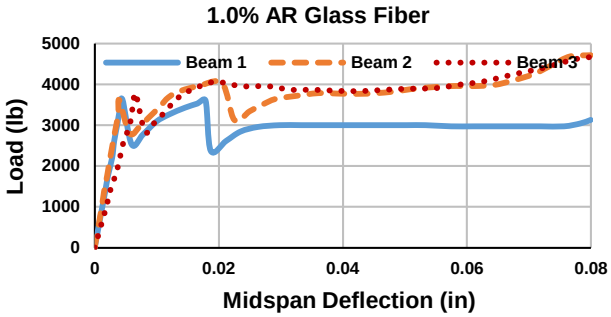

Shafei et al. 2018, Bridge Engineering Center

Figure 11. Flexural strength testing results for mixture containing 1.0% AR glass fibers

As illustrated in Figure 11, first peak strength describes a material's flexural capacity prior to crack formation, while toughness describes the area under the load-deflection curve.

The main observations were as follows:

- First peak strength was not significantly affected by fiber type or volume (Figure 12).

- Toughness was increased by increasing the fiber volume percentage for all the tested fibers. The highest toughness was provided by AR glass fibers, followed by PP and PVA fibers (Figure 13).

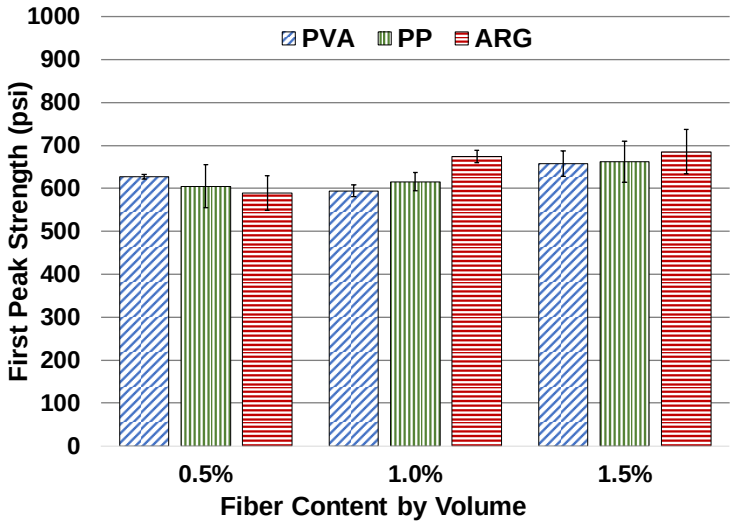

Shafei et al. 2018, Bridge Engineering Center

Figure 12. First peak strength for mixtures containing different fiber types and volumes

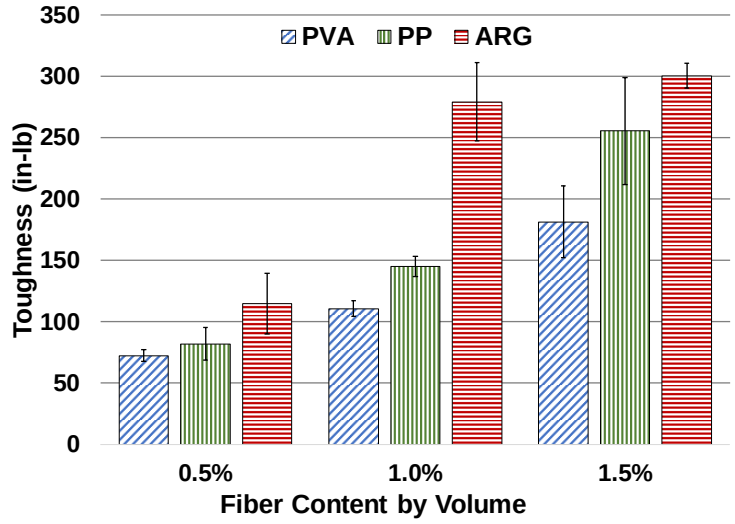

Shafei et al. 2018, Bridge Engineering Center

Figure 13. Toughness for mixtures containing different fiber types and volumes

It is interesting to note that the first peak strength trends are opposite for mixtures with 0.5% fiber content compared to mixtures with 1.0% and 1.5% fiber contents. This could be due to dispersion issues with the PVA and high-strength polyethylene (HSPE) at higher volumes, forming weak spots in the cross section. However, the 1.5% PVA mixtures showed relatively high first peak strengths despite fiber clumping issues.

Embedded Reinforcement

The role of embedded reinforcement in link slabs can be summarized as follows:

- Link slabs provide continuity over the piers. Thus, unlike the rest of the deck, link slabs often experience notable tensile stresses under flexure.

- The reinforcement embedded in link slabs is intended to resist the negative moment and keep the cracking width below the code-specified limits (Figure 14).

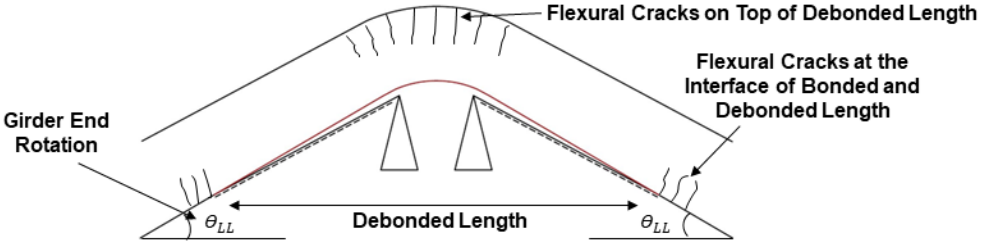

After Ho and Lukashenko 2011

Figure 14. Areas of cracking in link slabs

Nonmetallic reinforcement materials such as fiber-reinforced polymer (FRP) products can be used instead of steel rebar in link slab reinforcement (Figure 15). These materials have the following advantages:

- Nonmetallic (i.e., noncorrosive)
- High strength
- Light weight

Shafei. Bridge Engineering Center

Figure 15. Nonmetallic reinforcement before concrete placement

Figures 16 and 17 illustrate the characteristics of GFRP rebar.

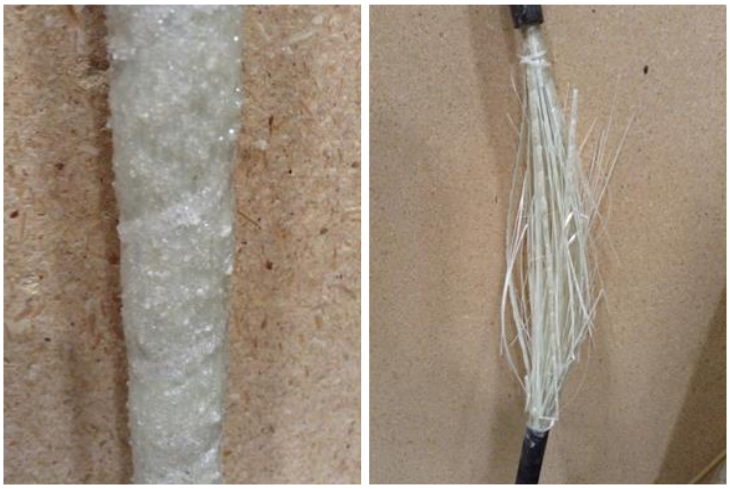

Shafei et al. 2020

Figure 16. GFRP rebar before (left) and after (right) failure

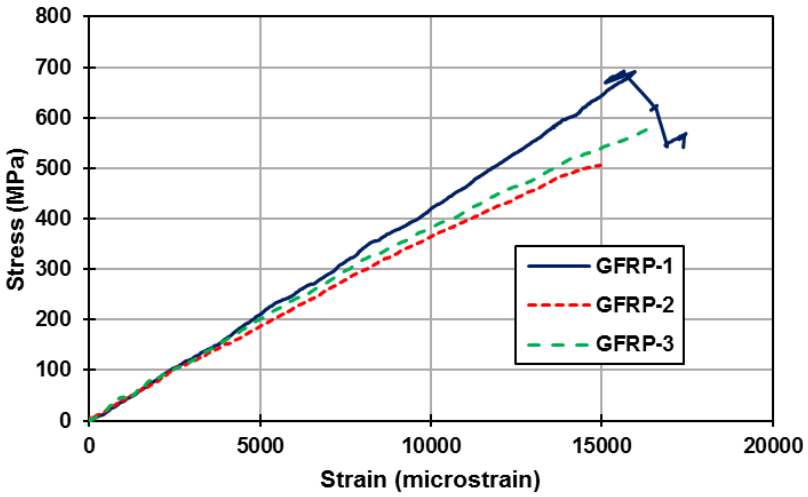

Shafei et al., Bridge Engineering Center

Figure 17. Stress versus strain for GFRP rebar

DESIGN CONSIDERATIONS

Design of Link Slabs According to Caner and Zia 1998

The main assumptions of the design methodology by Caner and Zia (1998) are as follows:

- Girders underneath the link slab are simply supported.
- No rigidity is induced by the link slab.
- The target end rotation due to live load (θ_{LL}) is determined from structural analysis based on the uncracked properties of the deck and the girder.

These assumptions are illustrated in Figure 18.

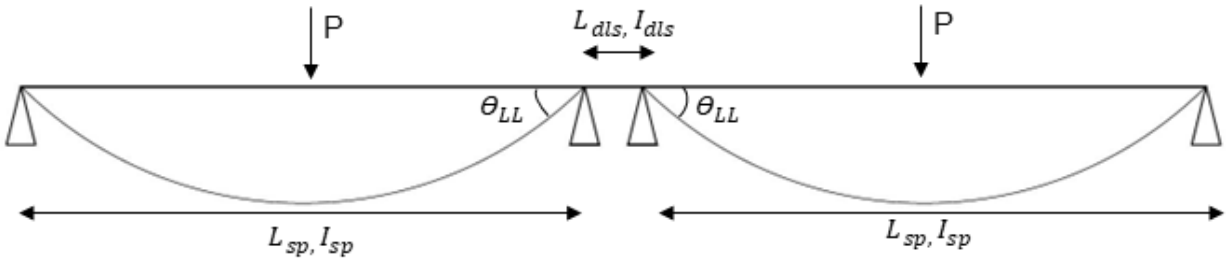

Figure 18. Assumptions of the design methodology by Caner and Zia 1998

The target end rotation is employed to find the end live load moment capacity by the following equation:

$$M_{LL} = \frac{2E_c I_{ls} \theta_{LL}}{L_{dls}}$$

where

M_{LL} = moment induced by end rotation
E_c = link slab's elastic modulus
I_{ls} = link slab's gross moment of inertia
L_{dls} = link slab's debonded length

Using the M_{LL} moment, the required steel rebar area is calculated, following the conventional reinforced concrete (RC) design equations available for rectangular cross sections (Figure 19).

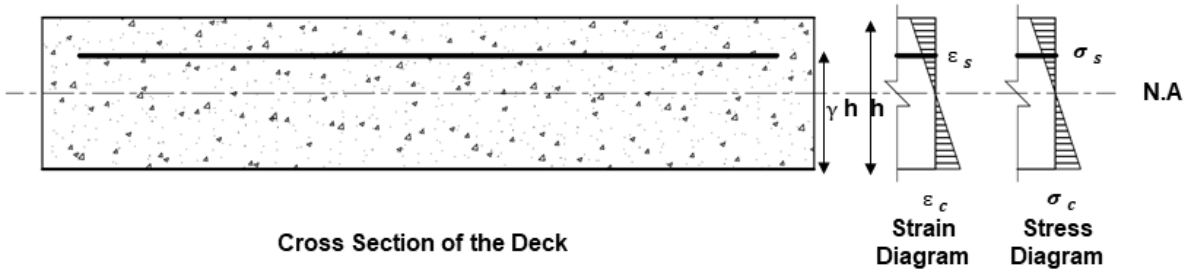

Figure 19. Bridge deck cross section and stress and strain diagrams

The strain and stress in embedded rebars are also calculated for serviceability checks.

Serviceability Control

To meet serviceability requirements, the crack width must remain less than 0.013 in. Thus, the crack width control criterion, z, is checked:

$z = f_s(d_c A)^{1/3}$ < 130 kip/in. for severe exposure and 170 kip/in. for moderate exposure

where f_s = stress in steel, which has to be less than $0.4f_y$, in which f_y is the steel's yield strength; d_c = depth of rebars from the compression face; and A = effective area around each rebar.

The crack width can be, alternatively, predicted from the following equation:

$$\omega = 0.076\beta f_s(d_c A)^{1/3}$$

where β = distance from the tension face to the neutral axis divided by the distance from the steel centroid to the neutral axis.

Expected Loads

Further to the consideration of rotations due to live loads, the design of link slabs should consider *temperature-induced rotations* and *rotations from the combined effect of creep and shrinkage*.

The corresponding end rotations can be obtained from *AASHTO LRFD Bridge Design Specifications* for (1) temperature effects, and (2) shrinkage and creep effects.

According to a field study conducted by Wing and Kowalsky (2005), the temperature-induced rotations can exceed those due to live loads. If this is observed to be the case, the design process should be checked and repeated (if needed).

Design of Link Slabs According to Okeil and ElSafty 2005

Okeil and ElSafty (2005) modified the three-moment equation to more accurately determine the moments experienced by link slabs, depending on their support conditions. The proposed methodology considers two support conditions:

- Both supports under the link slab are pinned, while the end supports are rollers (Figure 20, left).

- Both supports under the link slab are roller, while the end supports are pinned (Figure 20, right).

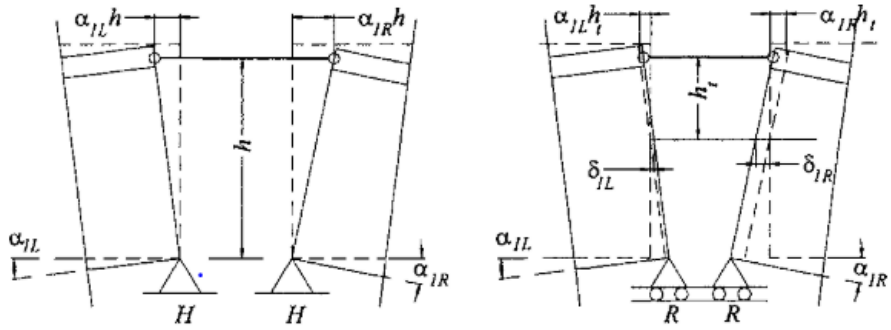

Okeil and ElSafty 2005, ©ASCE 2005, used with permission

Figure 20. Pinned supports under the link slab (left) and roller supports under the link slab (right)

Three-Moment Equation

The base three-moment equation:

$$M_0 \frac{L_L}{(EI)_L} + 2M_1 \left[\frac{L_L}{(EI)_L} + \frac{L_R}{(EI)_R}\right] + M_2 \frac{L_R}{(EI)_R} = -6\left[\frac{r_{1L}}{(EI)_L} + \frac{r_{1R}}{(EI)_R}\right]$$

Modified equation for two pin supports under the link slab:

$$M_0 \frac{L_L}{E_g I_{gL}} + 2M_1 \left[\frac{L_L}{E_g I_{gL}} + \frac{L_R}{E_g I_{gR}} + 3\frac{L_{link}}{h^2 E_s I_s}\right] + M_2 \frac{L_R}{E_g I_{gR}} = -6\left[\frac{r_{1L}}{E_g I_{gL}} + \frac{r_{1R}}{E_g I_{gR}}\right]$$

Modified equation for two roller supports under the link slab:

$$M_0 \frac{L_L}{E_g I_{gL}} + 2M_1 \left[\frac{L_L}{E_g I_{gL}} + \frac{L_R}{E_g I_{gR}} + 3\frac{3}{h^2}\left(\frac{L_L}{E_g A_{gL}} + \frac{L_R}{E_g A_{gR}} + \frac{L_{link}}{E_s A_s}\right)\right] + M_2 \frac{L_R}{E_g I_{gR}} = -6\left[\frac{r_{1L}}{E_g I_{gL}} + \frac{r_{1R}}{E_g I_{gR}}\right]$$

Calculation of Moment Demand

The following parameters, illustrated in Figure 21, are used in three-moment equations:

- M_0 = moment at the left end of Span 1
- M_1 = continuity moment
- M_2 = moment at the right end of Span 2
- L_L = left span's length
- L_R = right span's length
- L_{link} = link slab's length
- $E_g I_{gL}$ and $E_g I_{gR}$ = flexural rigidity of left and right span, respectively
- $E_s I_s$ = link slab's flexural rigidity
- r_{1L} and r_{1R} = reaction forces
- h = distance from the bottom of the girder to the link slab's centroid

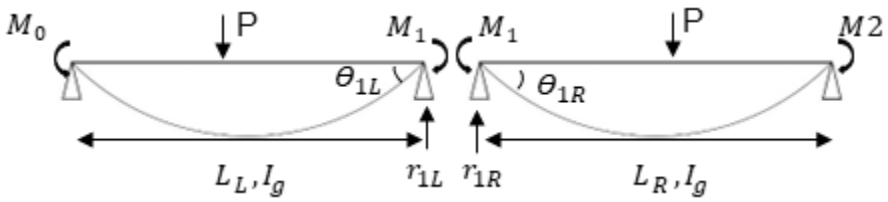

Figure 21. Parameters used in three-moment equations

Design Example 1

Scenario and Parameters

Design a link slab for a bridge with AASHTO type IV girder under the combined loading of dead load, lane load of 0.64 k/ft, and HL-93 truck load with impact.

The bridge properties are as follows:

- Span length = 60 ft
- Expansion joint = 2 in. (usually in the range of 1 to 3 in.)
- Concrete's compressive strength = 6.5 ksi
- Steel's modulus of elasticity = 29,000 ksi
- Width of deck (and link slab) = 12 ft
- End rotation = 0.0034 rad

The bridge properties are illustrated in Figure 22, and an AASHTO Type IV girder modeled in SAP2000 is shown in Figure 23.

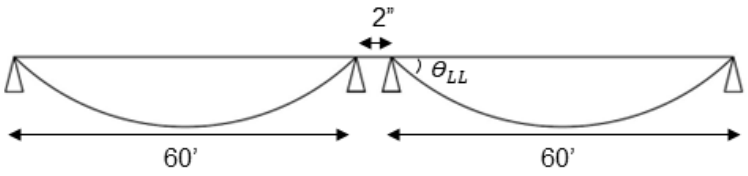

Figure 22. Bridge properties in Design Example 1

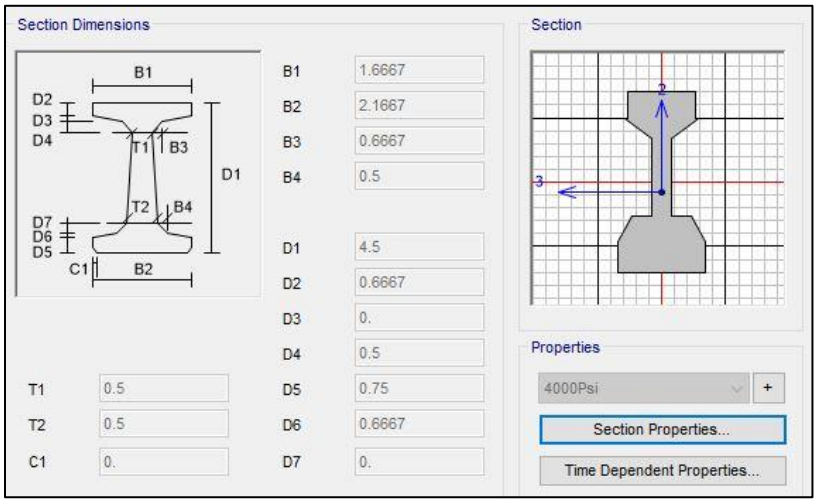

Figure 23. AASHTO Type IV girder modeled in SAP2000

The end rotation values are determined at girder ends, assuming girders are simply supported. A structural analysis software product, e.g., SAP2000 or RISA 2D/3D, can be used for this purpose.

The structural analysis setup includes the deck and the girder. The end rotation under dead load, service load for HL-93 truck, and lane load is obtained.

A link slab's unit section has a 12 in. width with a depth equal to the deck's depth. The link slab's main reinforcement is provided at the top of the section. The link slab section and strain distribution are illustrated in Figure 24.

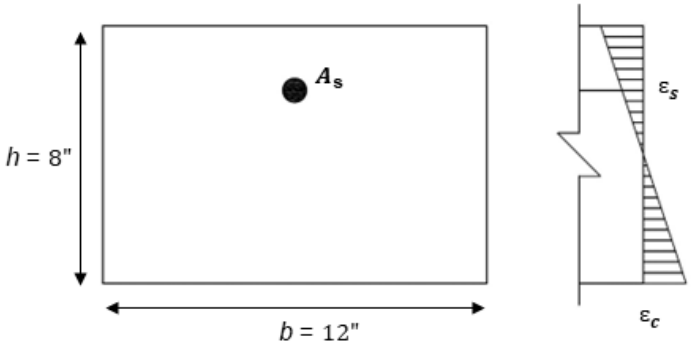

Figure 24. Link slab section (left) and strain distribution (right)

Steps and Calculations

Step 1. Determine the required properties.

- $E_c = 57000\sqrt{f_c'}$ = 4,595,487 psi = 4,595.5 ksi
- $f_r = 7.5\sqrt{f_c'}$ = 605 psi = 0.605 ksi

Step 2. Determine the debonded length.

The commonly recommended debonded length is 5%.

- Debonded Length = L_{dls} = (5% of span length) × 2 + expansion joint
- Debonded Length = 0.05 × (2 × 60 × 12) + 2 = 74 in

Step 3. Determine the link slab's gross moment of inertia.

- $I_{ls} = I_g = \frac{bh^3}{12} = \frac{12 \times 8^3}{12}$ = 512 in^4

Step 4. Determine the applied moment.

- $M_a = \frac{2E_c I_{ls} \theta_{LL}}{L_{dls}} = \frac{2 \times 4595.5 \times 512 \times 0.0034}{74}$ = 216.2 kip.in = 18.01 kip.ft

Step 5. Determine the cracking moment.

- $M_{cr} = \frac{f_r I_g}{y} = \frac{0.605 \times 512}{(\frac{8}{2})}$ = 77.44 kip.in = 6.45 kip.ft

Step 6. Determine the ratio of M_{cr}/M_a.

- $M_{cr}/M_a = \frac{6.45}{18.01}$ = 0.35

This can be used to directly evaluate f_s.

Step 7. Select a trial rebar size and spacing.

Try #8 rebars at 5 in. center-on-center (c/c) spacing.

- $\rho = \frac{\text{Area of rebar}}{\text{spacing} \times \gamma h} = \frac{0.79}{5 \times 6}$ = 0.0263

- $n = \frac{E_s}{E_c} = \frac{29000}{4595} = 6.31$

Step 8. Find the stress in embedded rebars (f_s).

Use the equation below:

- $M_a = {f_s}/{f_r} \, (6M_{cr}\rho\gamma^2\{1 + \frac{n\rho}{3} - 0.333\sqrt{[(n\rho)^2 + 2n\rho]}\})$
- f_s = 22.24 ksi < $0.4f_y$ = 0.4(60) = 24 ksi

This confirms that the stress in the rebars remains lower than the conservative yield strength considered. This can also help confirm that the crack width parameter determined using the obtained f_s will be than the threshold z value.

Step 9. Check the crack width.

- z = $f_s(d_cA)^{1/3}$=$f_s(d_c2y(\frac{b}{s}))^{1/3}$ (Figure 25)
- z = $22.24 \times (2 \times 2 \times 2 \times 12/5)^{1/3}$
- z = 59.50 kip/in. < 130 kip/in.

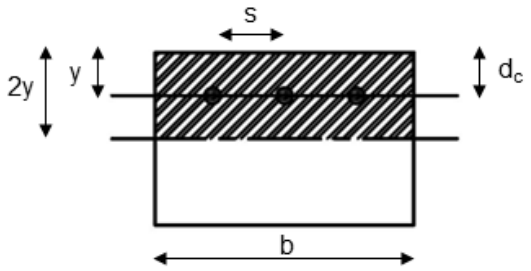

Figure 25. Crack width parameters

The design satisfies the crack width control criteria.

Step 10. Check that the design meets strength and serviceability requirements.

If the design does not meet either strength or serviceability requirements, Steps 7 through 9 should be repeated.

Check the design for temperature, shrinkage, and creep-induced rotations as well. If those rotations are higher than the rotations obtained for live loads, Steps 7 through 9 should be repeated.

Design Revision: Design of Link Slabs According to Au et al. 2013

The moment demand equation proposed by Caner and Zia (1998) was suggested to be modified to consider the relative movement of the girder and the link slab because of debonding. For this purpose, the following multiplier, α_r, was introduced:

$$\alpha_r = \frac{4}{(1+\frac{3e}{L_{dls}})}$$

where e is the support to support distance at the pier location under the link slab and L_{dls} is the link slab's debonded length.

Design Example 2

Scenario and Parameters

For the same link slab designed following the procedure proposed by Caner and Zia (1998), the design is modified to include the effect of the link slab's debonded length, following Au et al. (2013). The modified bridge properties are illustrated in Figure 26.

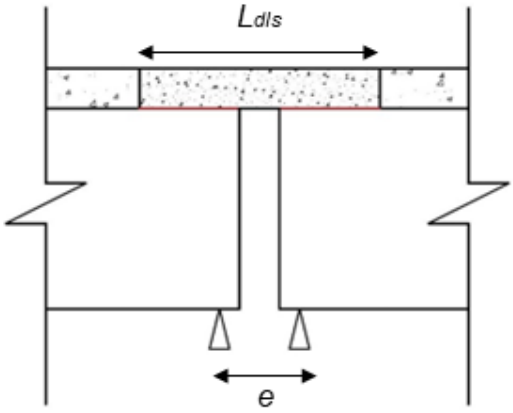

Figure 26. Modified bridge properties in Design Example 2

Steps and Calculations

Steps 1 through 3. The first three steps remain similar to those in Design Example 1.

Step 4. Determine the applied moment.

- $M_a = \frac{2E_c I_{ls} \Theta_{LL}}{L_{dls}} \alpha_r$
  where $\alpha_r = \frac{4}{(1+\frac{3e}{L_{dls}})}$

Assuming that the bearing pads are placed at 6 in. from the edge of the support:

- $e = 6 + 6 + 2 = 14$ in
- $\alpha_r = \frac{4}{(1+\frac{3e}{L_{dls}})} = \frac{4}{(1+\frac{3\times14}{74})} = 2.55$
- $M_a = \frac{2E_c I_{ls} \Theta_{LL}}{L_{dls}} \alpha_r = \frac{2\times4595.5\times512\times0.0034}{74} \times 2.55 = 551.34$ kip.in. = 45.95 kip.ft

Step 5. Determine the cracking moment.

- $M_{cr} = \frac{f_r I_g}{y} = \frac{0.605\times512}{(\frac{8}{2})} = 77.44$ kip.in. = 6.45 kip.ft

Step 6. Determine the ratio of M_{cr}/M_a.

- $M_{cr}/M_a = \frac{6.45}{45.95} = 0.14$

Step 7. Select a trial rebar size and spacing.

Try #11 rebars at 3.5 in. c/c spacing.

- $\rho = \frac{\text{Area of rebar}}{\text{spacing} \times \gamma h} = \frac{1.56}{3.5\times6} = 0.0743$
- $n = \frac{E_s}{E_c} = \frac{29000}{4595} = 6.31$

Step 8. Find the stress in embedded rebars (f_s).

Use the equation below:

- $M_a = {}^{f_s}/_{f_r} (6M_{cr}\rho\gamma^2\{1 + \frac{n\rho}{3} - 0.333\sqrt{[(n\rho)^2 + 2n\rho]}\})$
- $f_s = 21.54$ ksi $< 0.4f_y = 0.4(60) = 24$ ksi

This confirms that the stress in the rebars remains lower than the conservative yield strength considered.

Step 9. Check the crack width.

- $z = f_s(d_c A)^{1/3} = f_s(d_c 2y(\frac{b}{s}))^{1/3}$
- $z = 21.54 \times (2 \times 2 \times 2 \times 12/3.5)^{1/3}$
- $z = 57.71$ kip/in. < 130 kip/in.

The design satisfies the crack width control criteria.

Step 10. All design requirements are met.

A comparison between Design Example 1 and 2 shows that the steel required after the consideration of the link slab's debonded length can increase by up to two times. This highlights the need to appropriate structural analyses, paired with engineering judgement, to decide on the best design strategy for link slabs.

DETAILING REQUIREMENTS

The structural details are critical to ensure that the strength and durability of link slabs are maintained during the expected service life of bridges. Among the main structural details are debonded length, rebar material, and rebar spacing used in the link slab.

A set of laboratory tests was performed at Iowa State University to shed light on the contribution of the main design variables to the overall performance of link slabs (Shafei et al. 2018, Karim and Shafei 2021a). The laboratory testing setup is shown in Figures 27 and 28.

Figure 27. Link slab setup for laboratory testing

Figure 28. Exposed link slab reinforcement

Material and Geometric Properties of Laboratory Specimens

The material properties of the laboratory specimens were as follows:

- FRC for link slabs: f_c' = 7.5 ksi
- Embedded reinforcement: steel rebar in LS-1 and GFRP rebar in LS-2

The geometric properties were as follows:

- Steel girders: W21X55
- Two spans, each 21 ft
- Slab width: 63 in.
- Slab thickness: 8 in.

The material and geometric properties are illustrated in Figures 29 and 30.

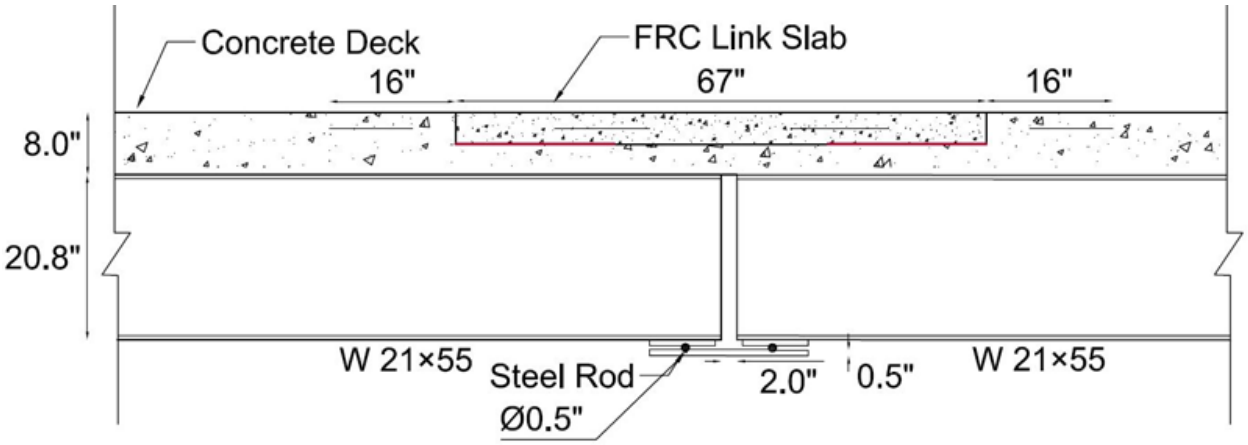

Figure 29. Diagram of laboratory link slab specimen

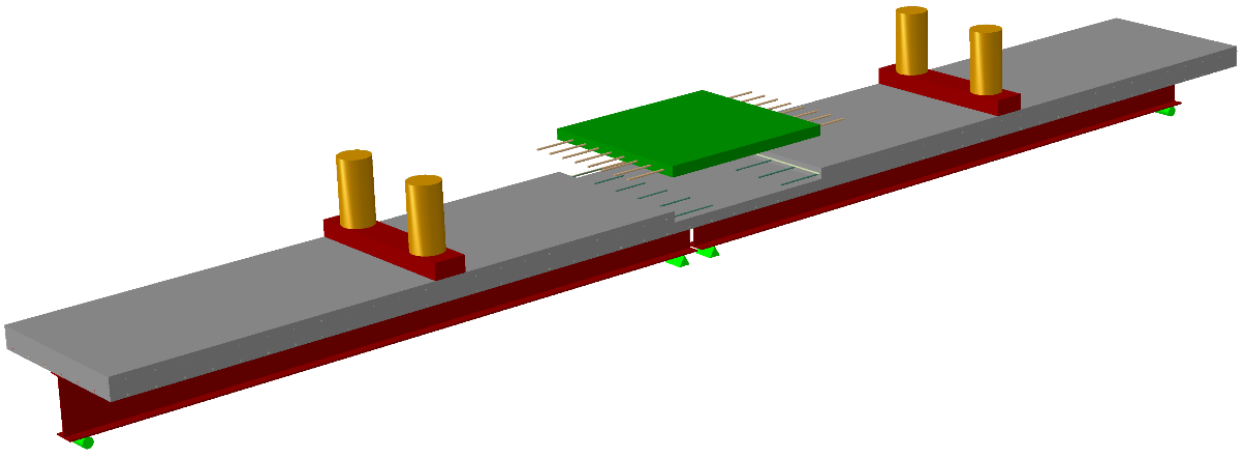

Figure 30. Three-dimensional rendering of laboratory link slab specimen

Construction of Laboratory Specimens

The steps involved in construction of the laboratory specimens are shown in Figures 31 through 34.

Figure 31. Steel girder surrounded by wooden framework to support a laboratory specimen

Figure 32. Wooden floor and form where laboratory specimen will be cast, with steel girder running through the center

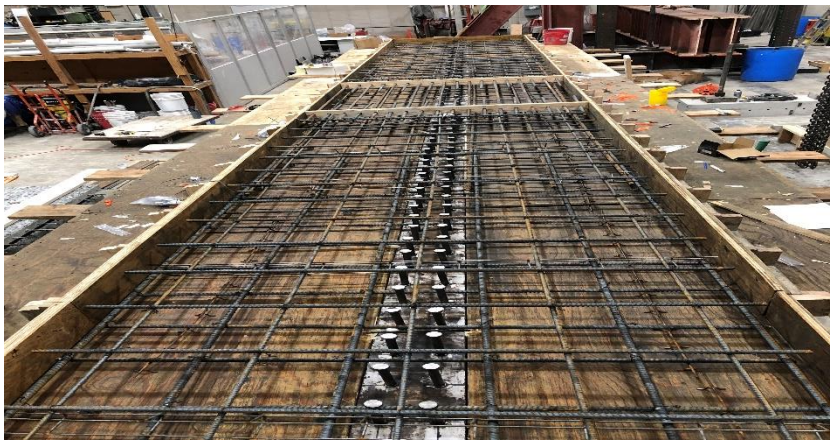

Figure 33. Steel reinforcement placed within the wooden form where laboratory specimen will be cast

Figure 34. Laboratory specimen with freshly poured concrete within the wooden forms

Reinforcement Details and Construction of Link Slabs

The reinforcement details of Link Slab 1 (LS-1) and Link Slab 2 (LS-2) are shown in Figures 35 and 36, respectively. LS-1 was reinforced with steel rebar, and LS-2 was reinforced with GFRP rebar. In both figures, the main rebar embedded in the link slabs is shown in blue, and the deck reinforcement is shown in green. In Figure 35, the supplementary rebars included in LS-1 are shown in red.

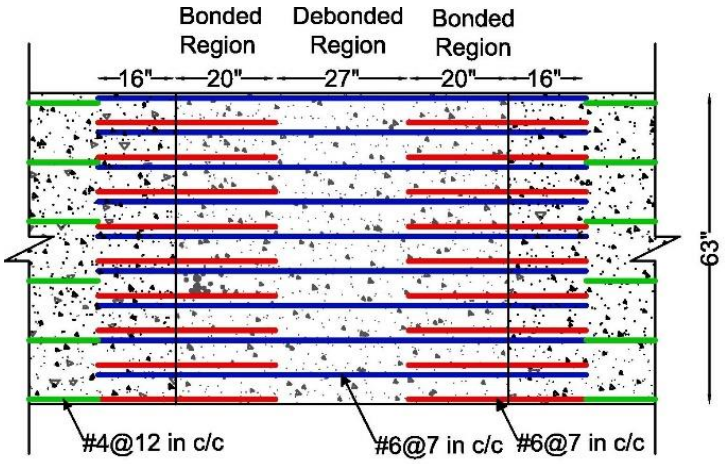

Figure 35. Steel rebar layout in LS-1

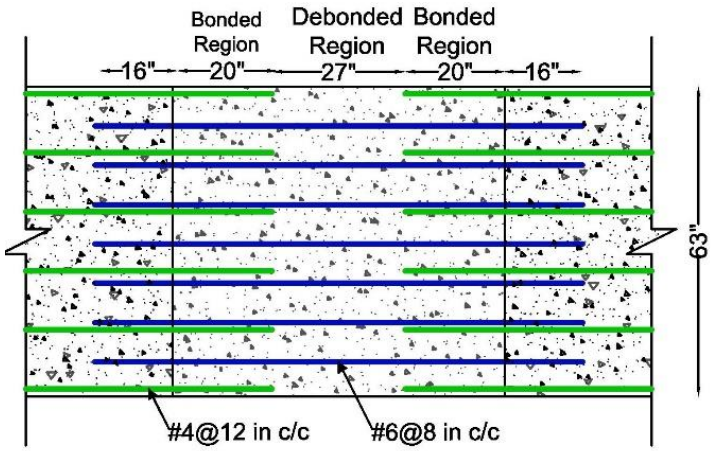

Figure 36. GFRP rebar layout in LS-2

During construction of both link slabs, dense instrumentation was included on the rebar and surface to capture all the strains in the rebar and on the face of the bonded and debonded regions.

The construction steps for LS-1 are shown in Figures 37 through 40.

Figure 37. Exposed rebar in LS-1 before construction

Figure 38. Instrumentation attached to rebar in LS-1

Figure 39. Freshly poured concrete in LS-1

Figure 40. Hardened concrete in LS-1 with patches marking instrumentation locations

The construction steps for LS-2 are shown in Figures 41 through 44.

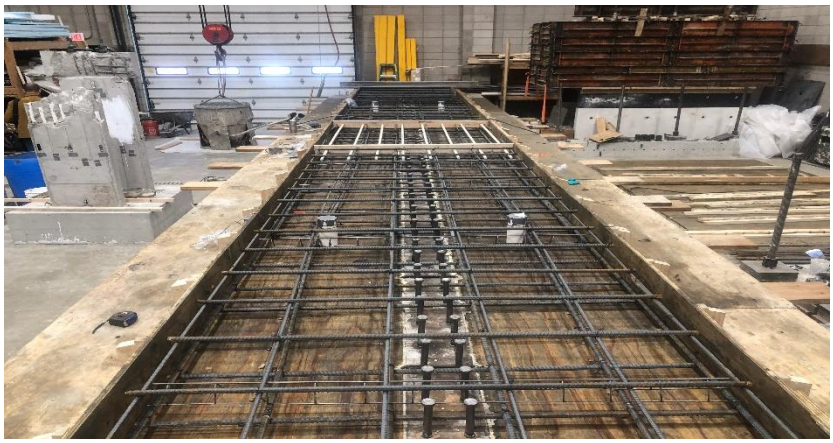

Figure 41. Wooden forms and rebar for second laboratory specimen before concrete pouring

Figure 42. Wooden forms and rebar for LS-2

Figure 43. Rebar for LS-2 after pouring adjacent slabs

Figure 44. Freshly poured concrete in LS-2

Both link slabs were loaded at the mid-span of each girder, as shown in Figure 45.

Figure 45. Link slab loading setup

Relationship between Load-Deflection and Strain

The load-deflection curves were found to follow a similar trend overall, as shown in Figure 46. At the maximum load, concrete crushing was noted under the two loading points, in addition to the formation and propagation of cracks in the link slab.

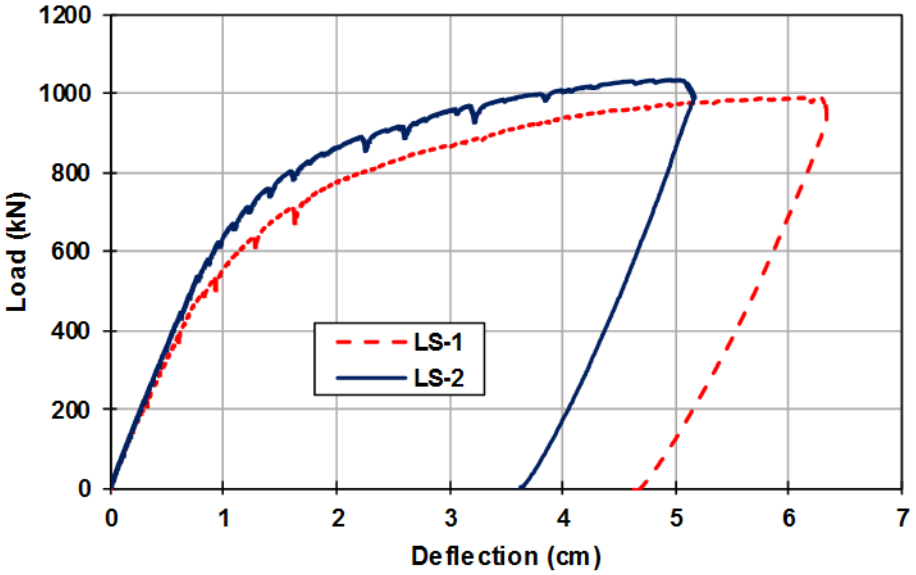

Figure 46. Load-deflection curves for LS-1 and LS-2

A comparison of strains generated in the bottom rebars of the concrete deck at the loading points highlights a smooth loading and unloading process in both link slabs, as shown in Figure 47.

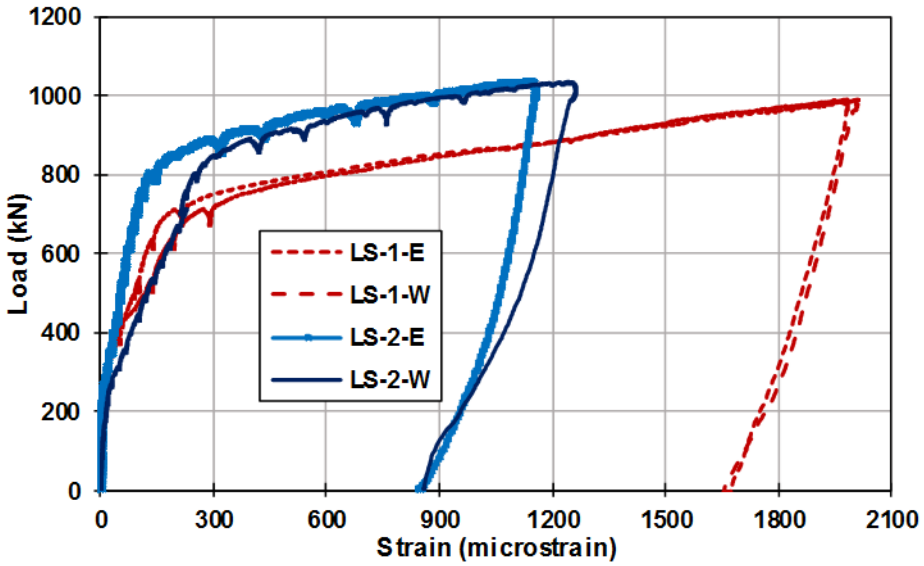

Figure 47. Load versus strain for LS-1 and LS-2 in the bottom rebar at the loading points

Under an external load of 444.8 kN (100 kip), in which the linear range ends, the steel rebars embedded in the debonded region of the LS-1 experience a strain of less than 700 microstrain, while the GFRP rebars embedded in the debonded region of the LS-2 undergo a strain of 3,000 microstrain (Figure 48).

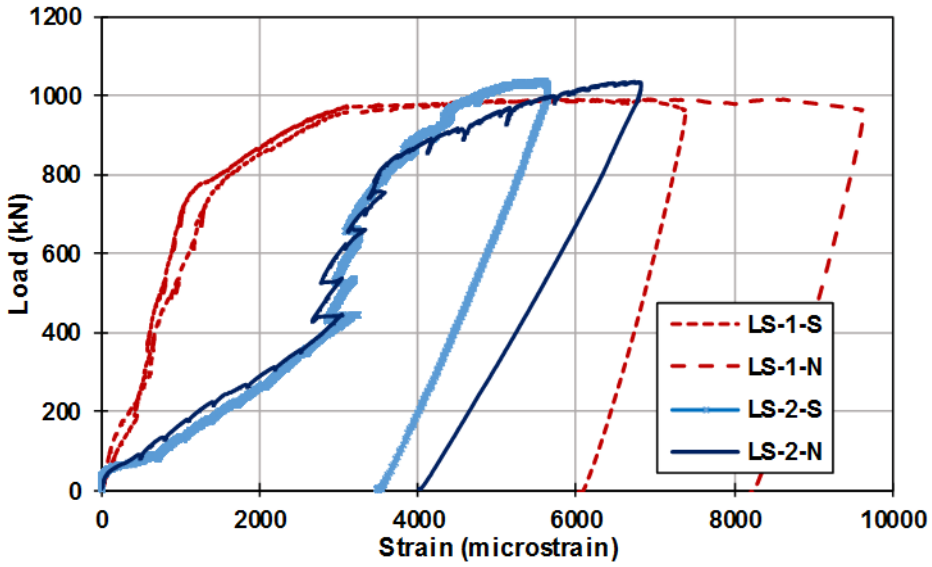

Figure 48. Load-strain curves obtained for the rebar in the debonded region

The comparison of strains, stresses, and forces clearly show how the embedded steel and GFRP rebar contribute to the load-bearing capacity of the link slabs.

It is noted that, under similar loading magnitudes, the GFRP rebar in LS-2 experiences smaller strains compared to the steel rebar in LS-1, given that the modulus of elasticity of GFRP is only a fraction of that of steel.

This observation highlights that the rebar in the bonded region of LS-1 experience greater stresses than the GFRP rebar in LS-2. This is further supported by the fact that LS-1 experienced higher deflections than LS-2.

Cracking Patterns

The crack patterns in LS-1 under ultimate load are shown in Figure 49.

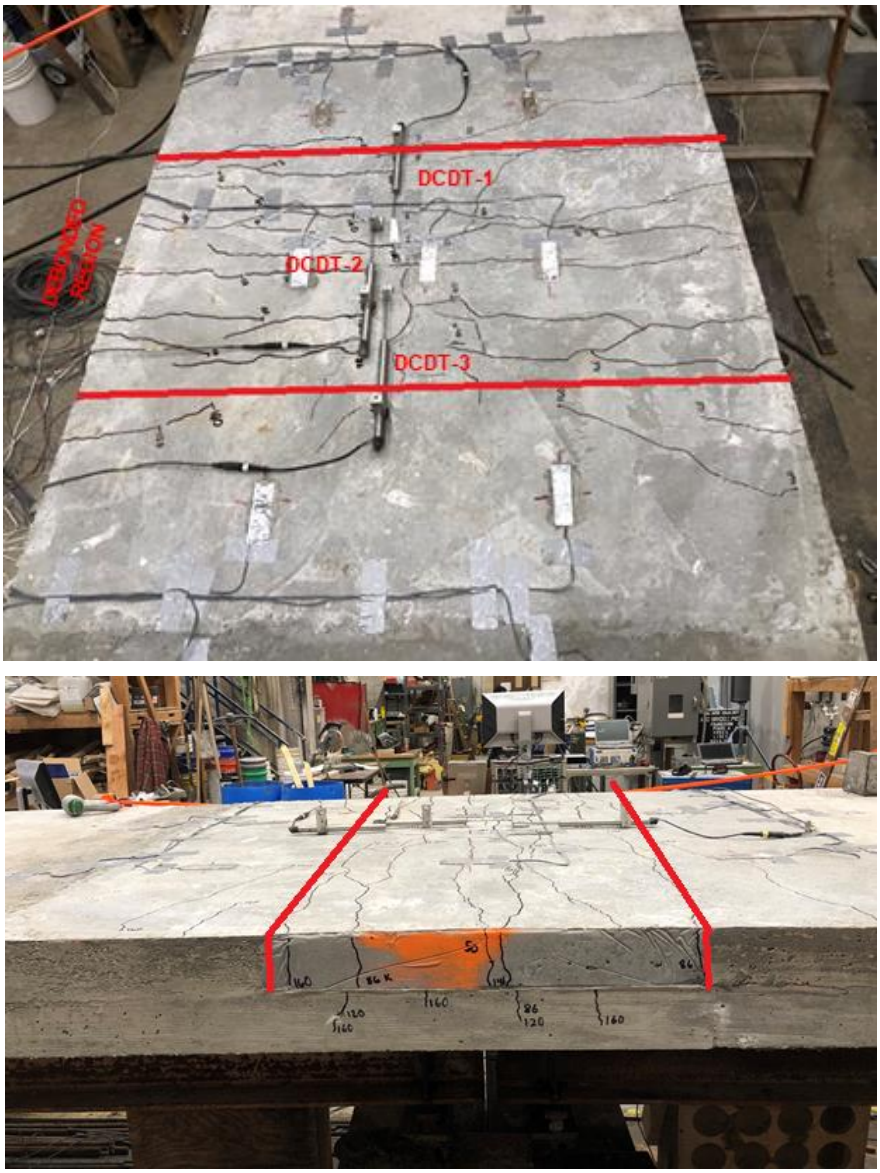

Figure 49. Crack patterns in LS-1: top view (top) and side view (bottom)

The crack patterns in LS-2 under ultimate load are shown in Figure 50.

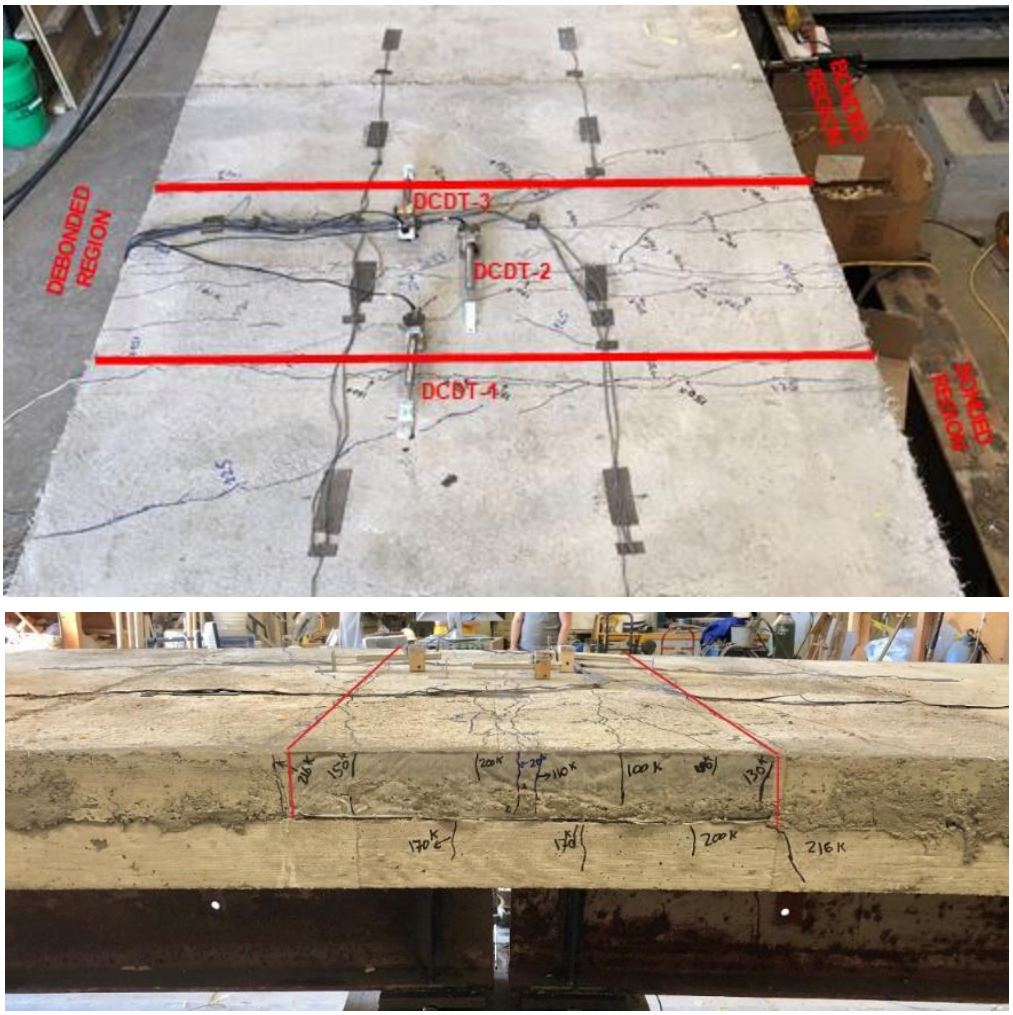

Figure 50. Crack patterns in LS-2: top view (top) and side view (bottom)

A comparison of crack widths revealed the following:

- The main cracks were formed in the debonded length of the tested link slabs.
- The first crack in LS-2 reached the AASHTO limit before the first crack in LS-1.

Cracks widths are compared in Figures 51 through 53.

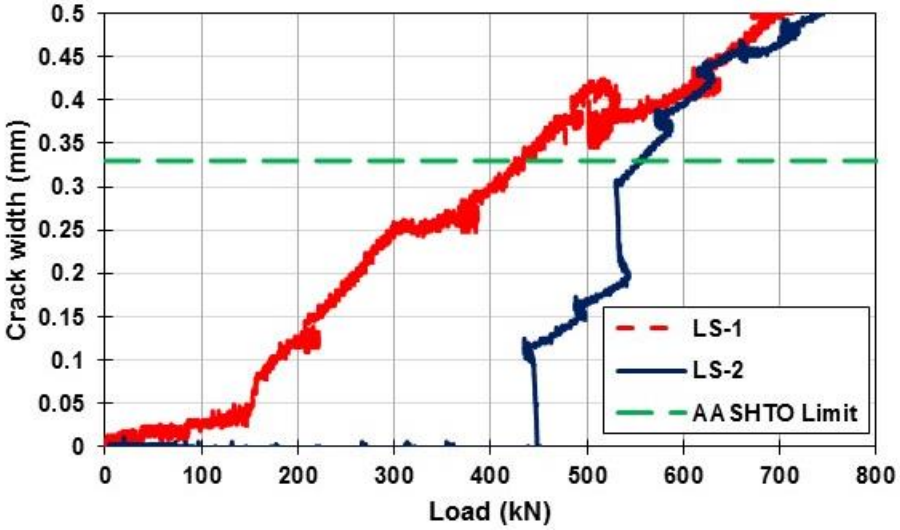

Figure 51. Crack width versus load in DCDT-1

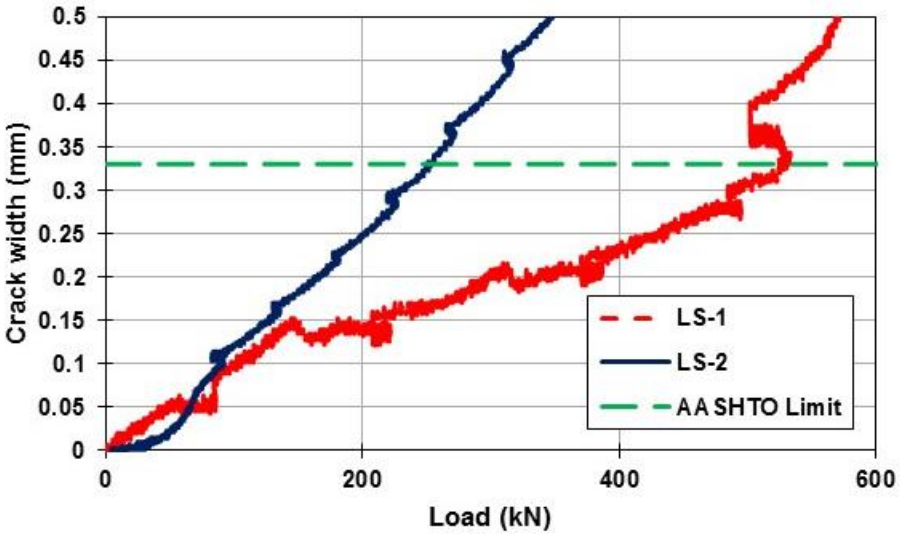

Figure 52. Crack width versus load in DCDT-2

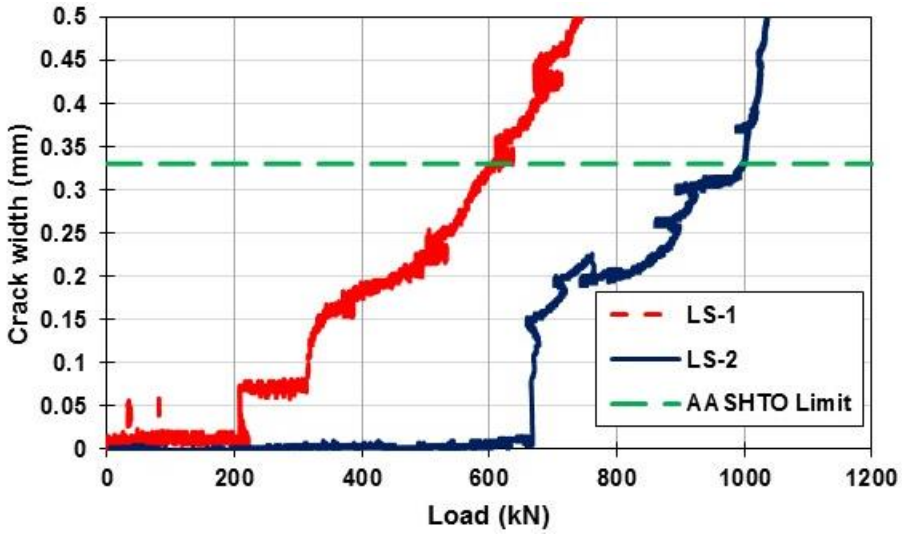

Figure 53. Crack width versus load in DCDT-3

Rebar Spacing

In link slabs, the rebar spacing is often decided such that the crack width remains less than the AASHTO-specified limit of 0.013 in.

From the finite element (FE) simulations reported in Karim and Shafei (2021a), strains in the link slabs with the maximum center-on-center rebar spacing were highest, while their variations became more pronounced as the magnitude of the applied load was increased. In particular, after the formation of first cracks, strains began to vary, depending on rebar spacing (Figure 54).

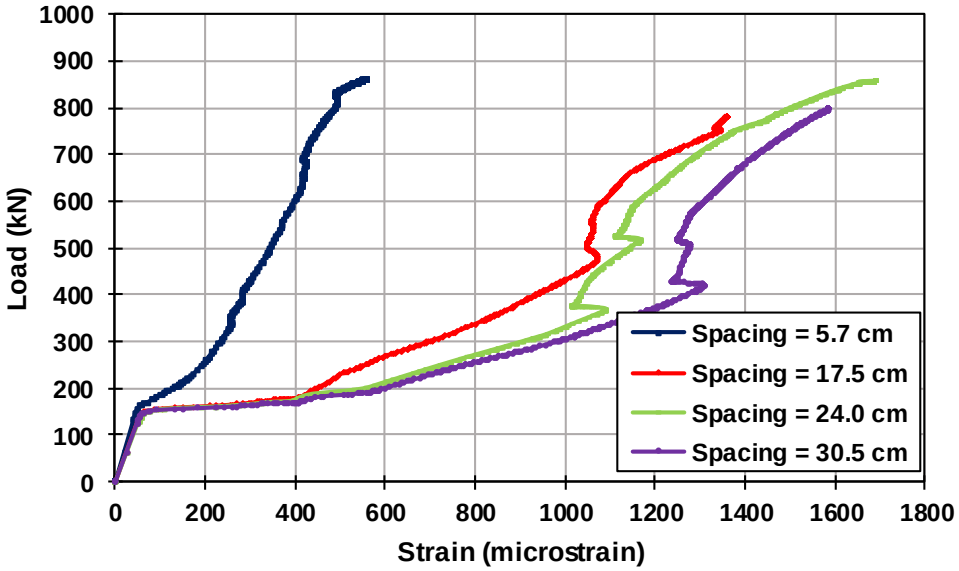

Figure 54. Load versus strain for various rebar spacings

ADDING LINK SLABS TO BRIDGES

Support Conditions

The consequences of adding link slabs to bridge structures can vary, depending on support conditions underneath them. The support conditions can also result in variations in the demand that the individual link slabs experience themselves. This is a critical aspect, particularly because the condition of bearing pads placed under the girders (Figure 55) often witnesses a transition from a roller to a pinned connection, due to wear and tear over time.

Figure 55. Elastomeric bearing pad

The LS-1 test setup discussed in the previous chapter (Shafei et al. 2018, Karim and Shafei 2021a) was investigated at the service limit for the effect of support conditions. The loading procedure was as follows:

- The setup was loaded up to 20 kips at mid-span of both spans.
- After reaching 20 kips, the setup was unloaded.
- The elastic response was recorded for various support conditions, including RPPR, PRRP, and PRPR, where R stands for roller support and P stands for pin support (Figure 56).

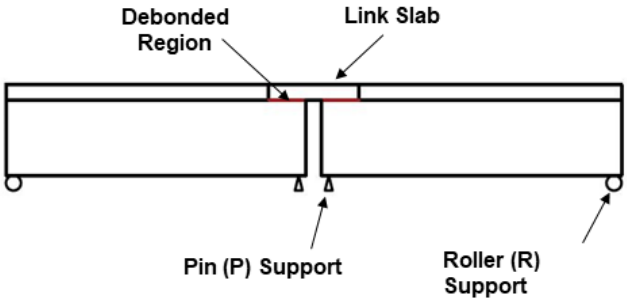

Figure 56. RPPR support configuration

An examination of the surface strains at the top of the debonded region revealed the following:

- All the load-strain curves were found to follow a similar trend, leading to a maximum strain in the range of 700 to 780 microstrain when the maximum load of 20 kip was reached.

- The RPPR support configuration presented the highest demand and the PRRP support configuration led to the lowest demand.

These findings are illustrated in Figure 57.

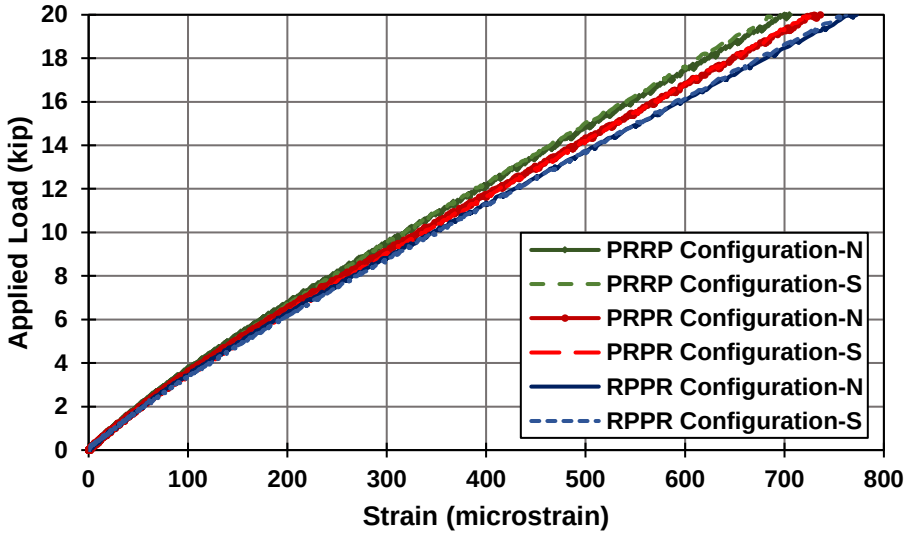

Figure 57. Applied load versus strain at the top of the debonded region for various support configurations

An examination of the strains in the rebar embedded in the debonded region revealed that the strains measured under the applied loads were consistently lowest for the PRRP support configuration and highest for the RPPR support configuration (Figure 58).

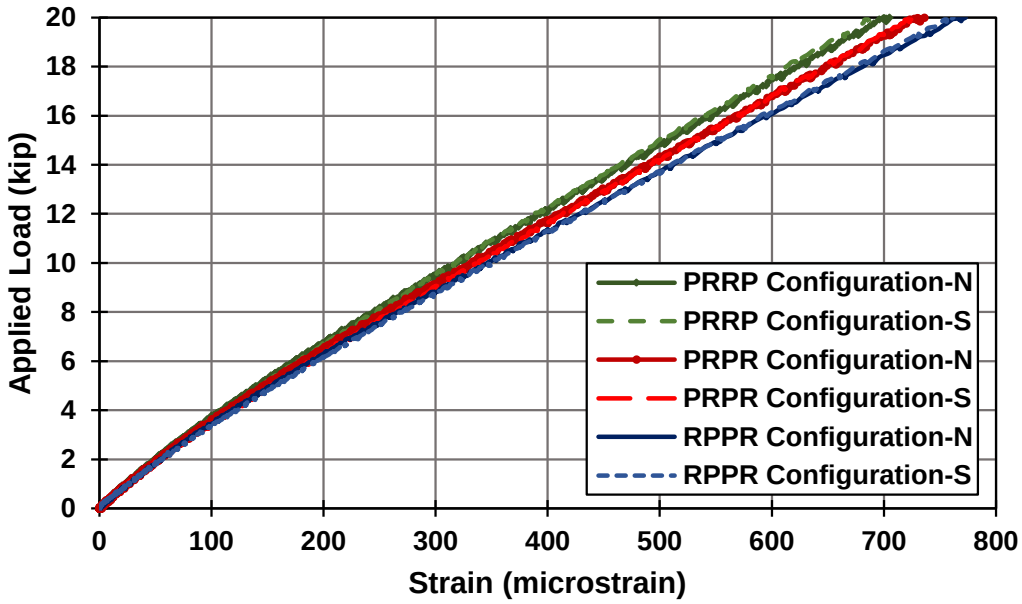

Figure 58. Applied load versus strain in the rebar embedded in the debonded region for various support configurations

Noting that the average maximum strain recorded in the top rebars changes from 140 to 230 microstrain, it is critical to design a link slab in such a way that the maximum strain can be accommodated without the formation of cracks, especially under service loads.

An examination of the vertical deflections revealed the following:

- With changing the support configuration from RPPR to PRRP, the maximum recorded deflection increases by up to 42%.

- The reported trend also indicates that the link slab setup with the RPPR support configuration provides the highest stiffness among the support configurations investigated in this study, while the PRRP support configuration provides the lowest stiffness.

These findings are illustrated in Figure 59.

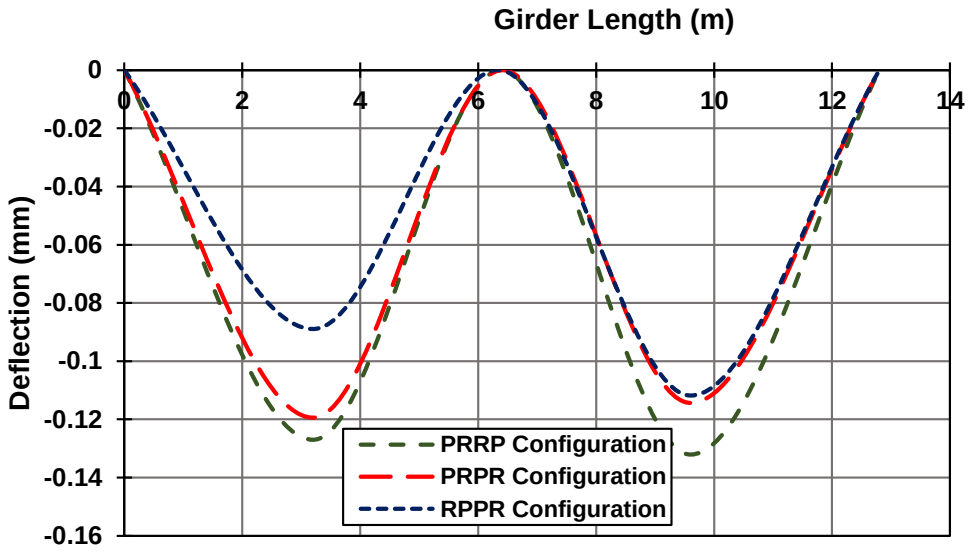

Figure 59. Vertical deflection versus girder length for various support configurations

This trend can be explained by the physical fact that the two pinned supports under the link slab in the RPPR support configuration do not move, and thus, directly contribute to increasing the setup's overall stiffness.

Full Bridge Structure

Bridge Model

To understand how the addition of link slabs can change the loading demand that bridge super and substructure components experience, a representative multi-span bridge was modeled and evaluated (Figure 60).

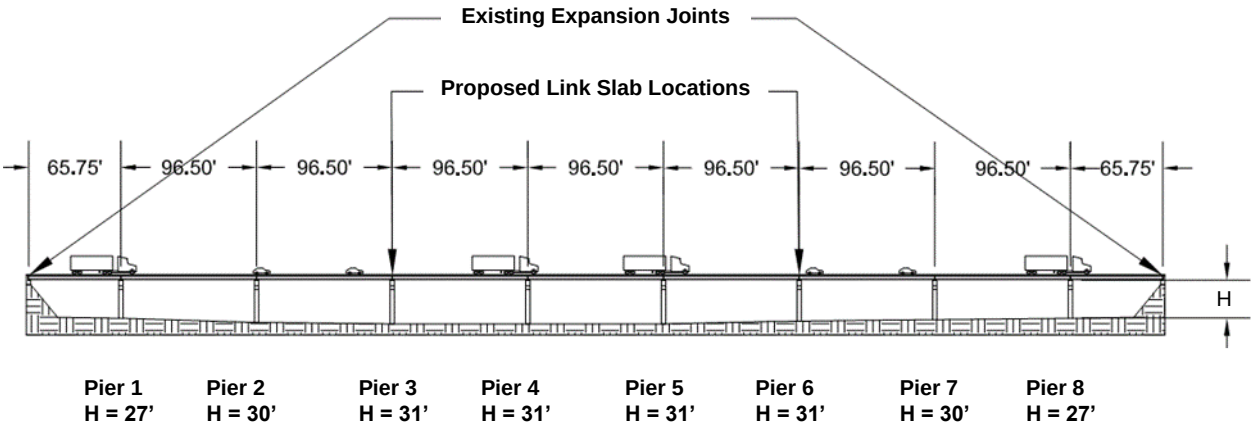

Figure 60. Diagram of modeled multi-span bridge

The bridge was modeled with the following features:

- Total length of 812 ft
- Nine spans
- Eight piers and four expansion joints
- Expansion joints at the abutments and above Piers 3 and 6
- Link slab proposed to be placed over Piers 3 and 6

A three-dimensional rendering of the bridge is shown in Figure 61.

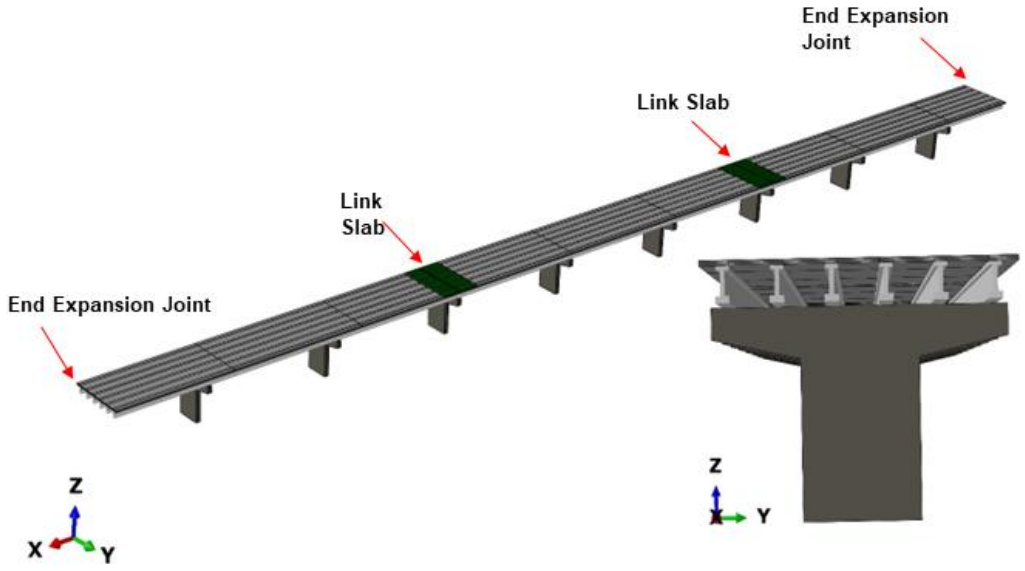

Figure 61. Three-dimensional rendering of the modeled bridge

Applied Loads and Simulations

The loads used in the evaluation were as follows:

- Dead load was accounted for the entire model.
- Based on a preliminary structural analysis, an HL-93 truck was placed at the locations that caused maximum moments in the link slabs.
- Temperature load captured a gradient of 50°F and 75°F.

The simulations used for the evaluation were as follows:

- Reaction forces and moments were determined at the base of the bridge piers.
- Bending moments and axial forces were estimated in the link slabs and in the deck.
- Comparisons were made between the bridge models with and without link slabs, taking into consideration various support configurations.

Link Slab Response

The following was found regarding the axial force in the link slab:

- For a debonded length of 2.5% and a temperature variation of 50°F, the axial force in the link slab was found to be maximum for the PRRP and PPPP support configurations and minimum for the RPPR support configuration.

- In the RPPR support configuration, the movements of the end rollers allow the release of the axial stresses, while in the PRRP and PPPP support configurations, the axial stresses developed in the superstructure is entirely transferred to the link slab.

These findings are shown in Figure 62.

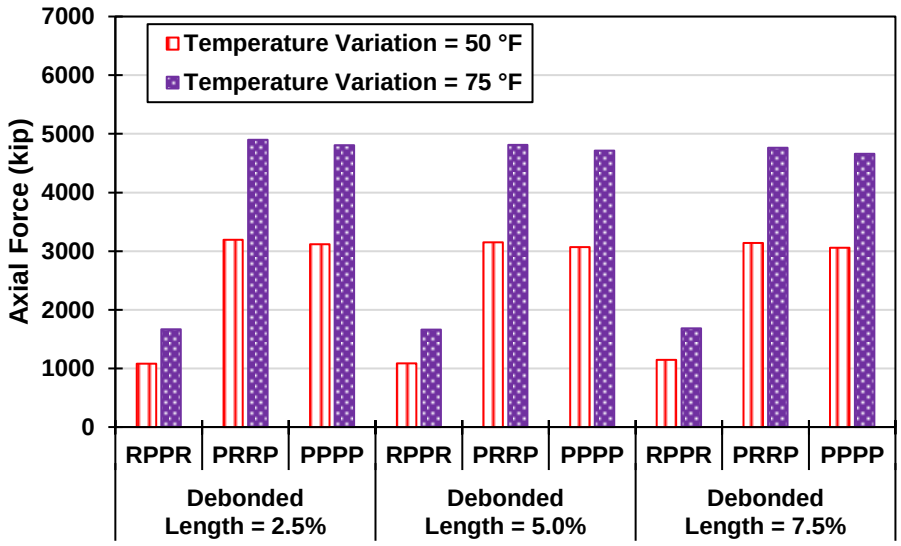

Figure 62. Axial force in the link slab for various support configurations, temperature variations, and debonded lengths

The following was found regarding the bending moment in the link slab:

- For the 2.5% debonded length, the PRRP and RPPR support configurations experienced the highest and lowest maximum bending moments under the 50°F temperature variation.

- With increasing the link slab's debonded lengths to 5.0% and 7.5%, however, the reported trend reverses, as the RPPR support configuration witnesses the highest maximum bending moment and the PRRP support configuration undergoes the lowest maximum bending moment.

These findings are shown in Figure 63.

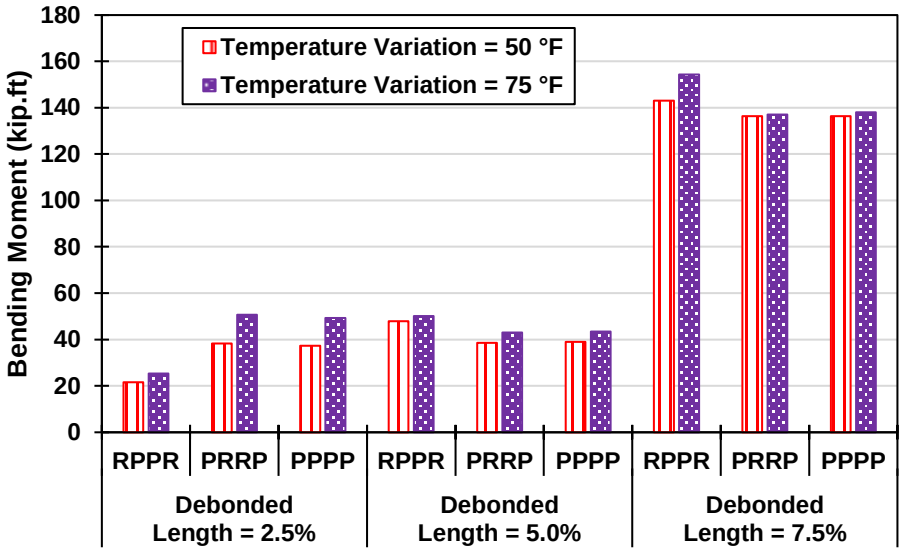

Figure 63. Bending moment in the link slab for various support configurations and temperature variations

The bridge's deflection profile for various support configurations is illustrated in Figure 64.

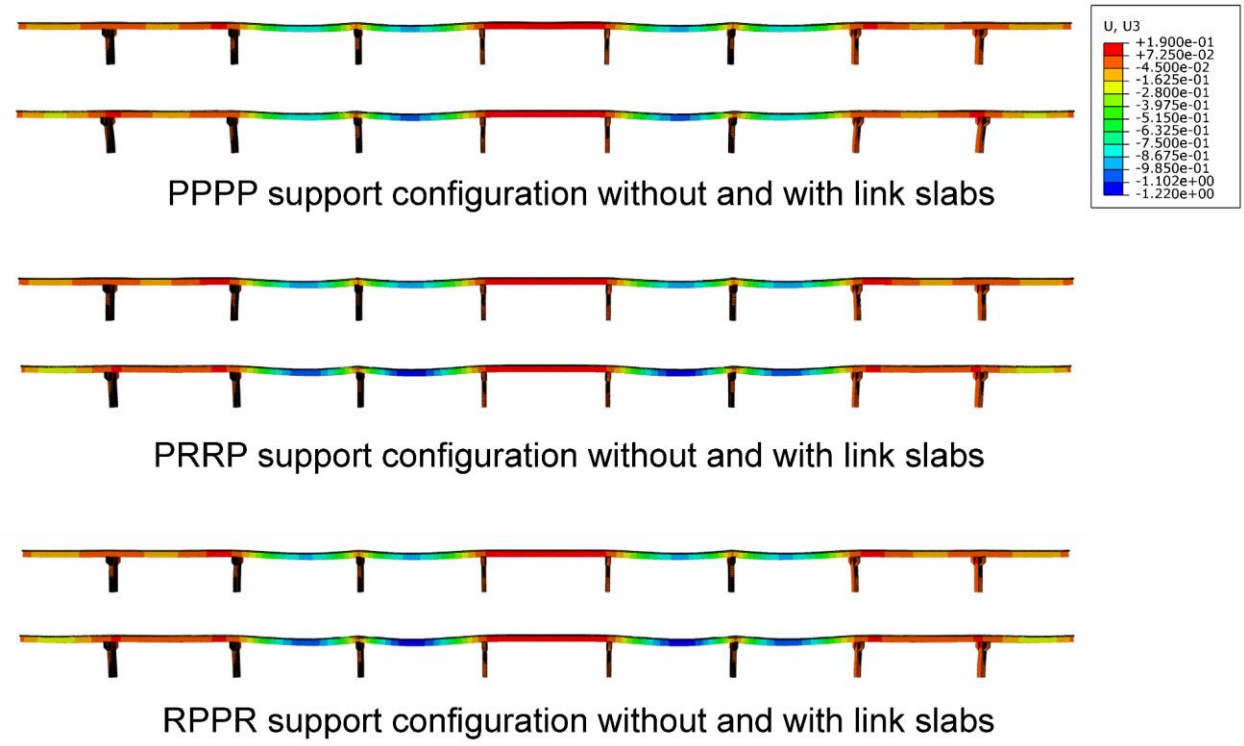

Figure 64. Bridge deflection profiles for three support configurations

Response of Substructure

The following responses were observed in the piers:

- The addition of link slabs results in an increase in the reaction moments generated in all the eight piers. The highest moments are generated in the end piers (i.e., Piers 1 and 8) for the RPPR support configuration.

- The highest increase in the reaction moments (i.e., by up to 11 times) is recorded in Piers 2 and 7 for the RPPR configuration.

- The reaction moments for the piers under the link slabs (i.e., Piers 3 and 6) are found to be maximum for the RPPR support configuration.

These findings are shown in Figure 65.

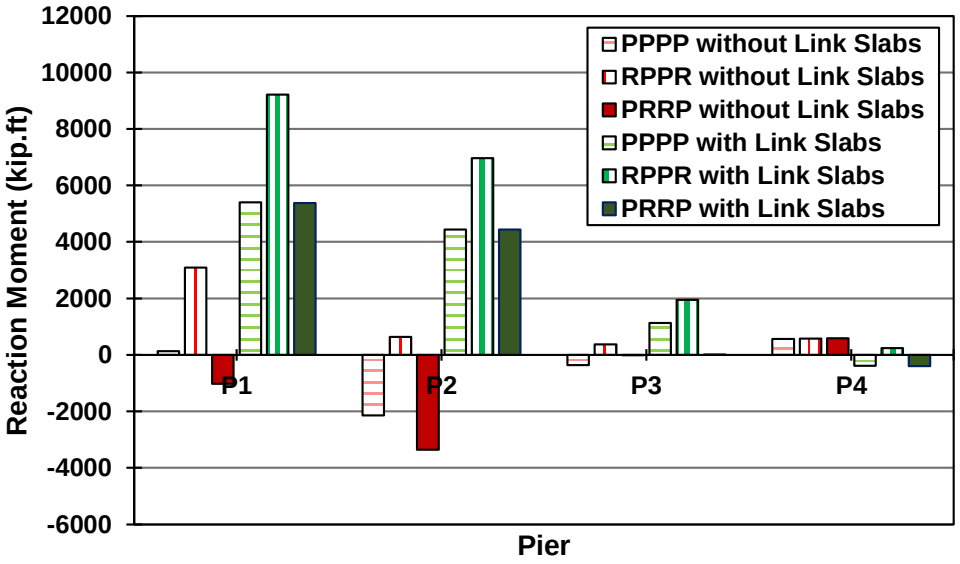

Figure 65. Reaction moment in piers with different support configurations

SUMMARY AND CONCLUSIONS

Selection of Materials

- The cementitious materials considered for link slabs include conventional concrete, FRC, ECC, and UHPC. For reinforcement materials, steel and GFRP rebars are the commonly-used choices.

- The cementitious material of choice for link slabs is expected to have the ability to experience multiple small cracks, while the maximum crack width is limited.

- The laboratory tests and field implementation of ECC link slabs have reported great performance. Similarly, the laboratory experiments on FRC link slabs have shown that desirable performance can be achieved with a good distribution of several narrow cracks. Field implemented UHPC link slabs have also been promising with no structural degradation during service.

- The GFRP rebars can be utilized in link slabs instead of steel rebars. Owing to their (relatively) high tensile strength and low elastic modulus, they can result in multiple, well-distributed cracks, further to offering appropriate corrosion resistance.

Design Considerations

- Beyond the choice of materials, the link slab's debonded length and rebar spacing are among the main design variables that need to be decided for maximum performance.

- The link slab's debonded length has been recommended to be 5% of its adjacent span length. A debonded length higher than 5% can result in a higher construction cost, while a debonded length lower than 5% can result in higher continuity moments.

- A combination of dead and live loads should be considered for the design of link slabs, following the code-specified requirements. Aspects associated with temperature-induced effects, as well as creep and shrinkage, should be also induced, especially for predicting end rotations.

- The rebar spacing is decided not only based on strength requirements but also taking into account crack width criteria. In particular, the rebar spacing should be sufficient to resist the girder's end moments generated by service loads.

Detailing Requirements

- The rebar spacing in the debonded region should be enough to keep the crack width below the code-specified limits. For example, AASHTO LRFD Bridge Design Specifications recommends a crack width of 0.012 in or the crack width parameter of z = 130 kip/in.

- The rebar spacing needs to meet the criteria for minimum rebar spacing to allow the flow of aggregates and vibrating equipment through the rebars.

- The transition from the deck to the link slab's debonded length is provided by a bonded region. Strategies, such as rebar extension, including dowels, and providing additional rebars, have been tested. Including dense rebars in this region has been found to be effective in keeping the connection between the link slab and the concrete deck intact with no macrocracks.

- The debonding necessary between the link slab and the concrete deck can be achieved by using a plastic sheet, while that between the deck and the steel girder is maintained by a roofing paper.

Adding Link Slabs to Bridges

- From the field surveys, it was found that superstructure supports can change from roller to pinned connections over time, mainly because of the wear and tear that the bearing pads undergo.

- The experimental tests and supporting numerical simulations have demonstrated that the support condition has a significant effect on the strains and stresses developed in link slab(s).

- The changes in the loading demand should be evaluated not only in superstructure but also in substructure components. This is critical to ensure that the combined effects of dead, live, and thermal loads are properly accommodated.

- A holistic investigation of the entire structure is necessary to ensure the safety and performance of all the bridge components, including link slab(s). This will maximize the advantages associated with the elimination of expansion joints, especially for long bridges.

REFERENCES AND SUPPLEMENTARY RESOURCES

Au, A., C. Lam, J. Au, and B. Tharmabala. 2013. Eliminating Deck Joints Using Debonded Link Slabs: Research and Field Tests in Ontario. *Journal of Bridge Engineering*, Vol. 18, No. 8, pp. 768–778.

Caner, A. and P. Zia. 1998. Behavior and Design of Link Slabs for Jointless Bridge Decks. *PCI Journal*, Vol. 43, No. 3, pp. 68–80.

Dopko, M., M. Najimi, B. Shafei, X. Wang, P. Taylor, and B. Phares. 2018. Flexural Performance Evaluation of Fiber Reinforced Concrete Incorporating Multiple Macro-Synthetic Carbon Fibers. *Transportation Research Record*: *Journal of the Transportation Research Board*, Vol. 2672, No. 27, pp. 1–12.

Graybeal, B. and F. Baby. 2013. Development of a Direct Tension Test Method for UHPFRC. *ACI Materials Journal*, Vol. 110, No. 2, pp. 177–186.

Ho, E. and J. Lukashenko. 2011. Link Slab Deck Joint. *Proceedings of the Annual Conference of the Transportation Association of Canada*, September 11–14, Edmonton, Alberta.

Karim, R. and B. Shafei. 2021a. Performance of Fiber-Reinforced Concrete Link Slabs with Embedded Steel and GFRP Rebars. *Engineering Structures*, Vol. 229, No. 111590, pp. 1–12.

Karim, R. and B. Shafei. 2021b. Flexural Response Characteristics of Ultra-High Performance Concrete Made with Steel Microfibers and Macrofibers. *Journal of Structural Concrete*, Vol. 22, No. 6, pp. 3476–3490.

Karim, R. and B. Shafei. 2022a. Addition of Partial-Depth Link Slabs to Bridge Structures: Role of Support Conditions. *Journal of Bridge Engineering*, Vol. 27, No. 7, 04022049, pp. 1–12.

Karim, R. and B. Shafei. 2022b. Investigation of Five Synthetic Fibers as Potential Replacements of Steel Fibers in Ultra-High Performance Concrete. *Journal of Materials in Civil Engineering*, Vol. 34, No. 7, 04022126, pp. 1–14.

Karim, R., M. Najimi, and B. Shafei. 2019. Assessment of Transport Properties, Volume Stability, and Frost Resistance of Non-Proprietary Ultra-High Performance Concrete. *Journal of Construction Building Materials*, Vol. 227, No. 117031, pp. 1–10.

Lárusson, L. H. 2013. *Development of Flexible Link Slabs using Ductile Fiber Reinforced Concrete*. PhD dissertation. Technical University of Denmark, Kongens Lyngby, Denmark.

Li. V. C. 2007. *Engineered Cementitious Composites (ECC) – Material, Structural, and Durability Performance*, University of Michigan, Ann Arbor, MI.

Li, V. C., G. Fischer, Y. Kim, M. Lepech, S. Qian, M. Weiman, and S. Wang. 2003. *Durable Link Slabs for Jointless Bridge Decks Based on Strain-Hardening Cementitious Composites*. University of Michigan, Ann Arbor, MI.

Li, V. C. and M. D. Lepech. 2009. *Application of ECC for Bridge Deck Link Slabs*. Materials and Structures, Vol. 42, No. 9, pp. 1185–1195.

Okeil, A. M. and A. ElSafty. 2005. Partial Continuity in Bridge Girders with Jointless Decks. *Practice Periodical on Structural Design and Construction*, Vol. 10, No. 4, pp. 229–238.

Royce, M. 2016. *Utilization of Ultra-High Performance Concrete (UHPC) in New York*. First International Interactive Symposium on UHPC, July 18–20, Des Moines, IA.

Russell, H. G. and B. A. Graybeal. 2013. *Ultra-High Performance Concrete: A State-of-the-Art Report for the Bridge Community*. FHWA-HRt-13-060. Federal Highway Administration, Turner-Fairbank Highway Research Center, McLean, VA.

Shafei, B., P. Taylor, B. Phares, M. Dopko, R. Karim, S. Hajilar, and M. Najimi. 2018. *Material Design and Structural Configuration of Link Slabs for ABC Applications*. Bridge Engineering Center at Iowa State University, Ames, IA. https://abc-utc.fiu.edu/wp-content/uploads/sites/52/2019/01/ISU-Link-Slab-Final-Report.pdf.

Shafei, B., B. Phares, and D. Saini. 2020. *Field Investigation of Bridge Deck Reinforced with Glass Fiber Reinforced Polymer (GFRP) Rebar*. Minnesota Department of Transportation Local Road Research Board, St. Paul, MN.

Shafei, B., M. Kazemian, M. Dopko, and M. Najimi. 2021. State-of-the-Art Review of Capabilities and Limitations of Polymer and Glass Fibers used in Fiber-Reinforced Concrete. *Journal of Materials*, Vol. 14, No. 409, pp. 1–44.

The Crittenden Press. 2012. https://crittendenpress.blogspot.com/.

Wing, K. M. and M. J. Kowalsky. 2005. Behavior, Analysis, and Design of an Instrumented Link Slab Bridge. *Journal of Bridge Engineering*, Vol. 10, No. 3, pp. 331–344.

Zia, P., A. Caner, and A. ElSafty. 1995. *Jointless Bridge Decks*. Center for Transportation Engineering Studies, North Carolina State University, Raleigh, NC.

THE INSTITUTE FOR TRANSPORTATION IS THE FOCAL POINT FOR TRANSPORTATION AT IOWA STATE UNIVERSITY.

InTrans centers and programs perform transportation research and provide technology transfer services for government agencies and private companies;

InTrans contributes to Iowa State University and the College of Engineering's educational programs for transportation students and provides K–12 outreach; and

InTrans conducts local, regional, and national transportation services and continuing education programs.

IOWA STATE UNIVERSITY

Visit **InTrans.iastate.edu** for color pdfs of this and other research reports.